



1 **Sedimentary record from the Canada Basin, Arctic Ocean:**
2 **implications for late to middle Pleistocene glacial history**

3 Linsen Dong^{1,2}, Yanguang Liu^{1,2}, Xuefa Shi^{1,2,*}, Leonid Polyak³, Yuanhui Huang^{1,2},
4 Xisheng Fang¹, Jianxing Liu^{1,2}, Jianjun Zou^{1,2}, Kunshan Wang^{1,2}, Fuqiang Sun¹, Xuchen
5 Wang⁴.

6 ¹Key Laboratory of Marine Sedimentology and Environmental Geology, First Institute of Oceanography, State

7 Oceanic Administration, Qingdao 266061, China

8 ²Laboratory for Marine Geology, Qingdao National Laboratory for Marine Science and Technology, Qingdao, 266

9 061, China

10 ³Byrd Polar and Climate Research Center, The Ohio State University, 43210, USA

11 ⁴Key Laboratory of Marine Chemistry Theory and Technology, Ocean University of China, Qingdao 266100,

12 China

13

14 *Corresponding author. Tel./fax: +86 532 88967491

15 E-mail address:xfshi@fio.org.cn(X.Shi)

16

17 **Abstract:** Sediment core ARC4–BN05 collected from the Canada Basin, Arctic
18 Ocean, covers the late to middle Quaternary (Marine Isotope Stages (MIS) 1-15, ca.
19 0.5-0.6 Ma) as estimated by correlation to earlier proposed Arctic Ocean
20 stratigraphies and AMS ¹⁴C dating of the youngest sediments. Detailed examination
21 of clay and bulk mineralogy along with grain size, content of Ca and Mn, and



22 planktonic foraminiferal numbers in core ARC4–BN05 provides important new
23 information about sedimentary environments and provenance. We use increased
24 contents of coarse debris as an indicator of glacier collapse events at the margins of
25 the western Arctic Ocean, and identify the provenance of these events from
26 mineralogical composition. Notably, peaks of dolomite debris, including large
27 dropstones, track the Laurentide Ice Sheet (LIS) discharge events to the Arctic Ocean.
28 Major LIS inputs occurred during the stratigraphic intervals estimated as MIS 3,
29 intra-MIS 5 and 7 events, MIS 8, and MIS 10. Inputs from the East Siberian Ice Sheet
30 (ESIS) are inferred from peaks of smectite, kaolinite, and chlorite associated with
31 coarse sediment. Major ESIS sedimentary events occurred in the intervals estimated
32 as MIS 4, MIS 6 and MIS 12. Differences in LIS vs. ESIS inputs can be explained by
33 ice-sheet configurations at different sea levels, sediment delivery mechanisms
34 (iceberg rafting, suspension plumes, and debris flows), and surface circulation. A
35 long-term change in the pattern of sediment inputs, with an apparent step change near
36 the estimated MIS 7/8 boundary (ca. 0.25 Ma), presumably indicates an overall
37 glacial expansion at the western Arctic margins, especially in North America.

38 **Keywords:** Sediment core, Pleistocene, western Arctic Ocean, clay minerals, bulk
39 minerals, sediment provenance, Laurentide Ice Sheet, East Siberian Ice Sheet

40

41 **1. Introduction**

42 The advances and decays of continental ice sheets play a significant role in the
43 alteration of global climatic system, such as changing atmospheric circulations,



44 creating large area albedo anomalies and regulating the global sea level fluctuations
45 (Clark et al., 1990). Reconstruction of the history of ice sheets is therefore important
46 not only for a better understanding of feedbacks of the future climate change and its
47 impact on regional climates, but also for getting insights into the mechanisms of
48 abrupt climate change.

49 Studies of Pleistocene glaciations around the Arctic Ocean dealt mostly with the
50 late Quaternary history of the Eurasian Ice Sheet during Marine Isotope Stages (MIS)
51 1–6 (e.g., Svendsen et al., 2004; Larsen et al., 2006) or the Laurentide Ice Sheet (LIS)
52 with a special attention to the Last Glacial Maximum (LGM) (e.g. Dyke et al., 2002;
53 England et al., 2009). In addition to terrestrial data, studies of sediment cores from the
54 Arctic Ocean are critical for comprehending the history of glacial advances and
55 retreats (e.g., Polyak et al., 2004; 2009; Spielhagen et al., 2004; Stein et al., 2012;
56 Kaparulina et al., 2015). However, the long-term history of circum-Arctic glaciations
57 is still poorly understood, especially with respect to the western Arctic including the
58 North America and East Siberia. While a major impact of the North American ice
59 sheets on circulation and depositional environments in the Arctic Ocean is indicated
60 by various marine and terrestrial data (e.g., Phillips and Grantz, 2001; Stokes et al.,
61 2005), the East Siberian Ice Sheet (ESIS) remained largely hypothetical until recently.
62 Some terrestrial and seafloor mapping data now provide evidence for the existence of
63 considerable ice masses on the East Siberian margin (Basilyan et al., 2010; Niessen et
64 al., 2013; Dove et al., 2014), but the timing and extent of these glaciations is virtually
65 unknown. Marine sedimentary records from the Arctic Ocean adjacent to the East



66 Siberian margin could add valuable information to this intriguing paleoglaciological
67 problem.

68 In this paper, we present a multiproxy study of glacial-interglacial changes
69 during the late to middle Pleistocene based on sediment core ARC4-BN05 from the
70 Canada Basin north of the Chukchi Plateau and east of the Mendeleev Ridge. This
71 location can be affected by the two main Arctic Ocean circulation systems, the
72 Beaufort Gyre and the Transpolar Drift, which carry sea ice, icebergs, and sediment
73 discharge from the North America and Siberia, respectively. As this circulation along
74 with sedimentary environments and sources varied greatly during the Pleistocene
75 climate cycles, resulting variations in sediment delivery and deposition make for a
76 valuable paleoclimatic record for the western Arctic. Biogenic proxies (such as
77 foraminifers) have uneven and overall limited distribution in Arctic Ocean sediments,
78 while the terrigenous component provides a more consistent material for
79 paleoceanographic studies (e.g. Stein, 2008; Polyak et al., 2009). As sediments in the
80 Arctic Ocean are primarily transported by sea ice and/or icebergs during glacial
81 events, sediment composition yields important information not only on the
82 provenance and transport pathways, but also on the attendant glacial and
83 paleoclimatic history (e.g. Spielhagen et al., 1997; Vogt et al., 2001; Knies et al.,
84 2001). By using clay and bulk mineralogy, along with grain size and the content of
85 major elements Ca and Mn, we reconstruct depositional environments and sediment
86 provenance to provide clues to the history of western Arctic ice sheets and their
87 interaction with the Arctic Ocean.



88

89 **2. Regional background**

90 The Arctic Ocean is surrounded by land masses composed of an assortment of
91 lithologies and situated in a variety of climatic, tectonic, and physiographic settings.
92 Figure 1 depicts a schematic geological map showing the main terrains and associated
93 lithologies (Fagel et al., 2014). The West Siberian Basin, East Siberian platform and
94 Verkhoyansk-Chukotka provinces of the Eurasian continent are mainly composed of
95 terrigenous sediment (Fagel et al., 2014). The Siberian (Putorana) traps constitute one
96 of the largest flood basalts in the world (Sharma et al., 1992). The western
97 Okhotsk-Chukotsk volcanic belt contains acidic to intermediate rocks, whereas
98 intermediate to basic rocks are more characteristic of the eastern side (Viscosi-Shirley
99 et al., 2003). The Kara Plate and the Taymyr foldbelt, as well as the Ural and Novaya
100 Zemlya foldbelt are mainly composed of intrusive and metamorphic rocks (Fagel et
101 al., 2014).

102 The geology of outcropping terraines of Alaska mainly includes
103 Canadian-Alaskan Cordillera, Brooks Range, and part of the Northern-American
104 platform containing mostly intrusive, metamorphic, and some clastic rocks (Fagel et
105 al., 2014). The outcrops of the Canadian Arctic Archipelago are mainly composed of
106 carbonate and clastic rocks (Phillips and Grantz, 2001; Fagel et al., 2014), whereas
107 intrusive and clastic rocks are mostly characteristic for Greenland (Fagel et al., 2014).

108 Dissolved and suspended matter is transported to the Arctic Ocean by
109 voluminous rivers, with the Lena and Mackenzie Rivers being the largest on the



110 Siberian and North American side, respectively. The transported material is further
111 distributed across the Arctic Ocean in water and/or ice by currents. The two main
112 surface, wind-driven circulation systems are the clockwise Beaufort Gyre (BG) in the
113 western Arctic and the Transpolar Drift (TPD) that carries water and ice from the
114 Siberian margin to the Norwegian-Greenland Sea (e.g., Rudels, 2009). The strength
115 and trajectories of these current systems may vary depending on changes in
116 atmospheric pressure fields known as the Arctic Oscillation (Rigor et al., 2002).

117 Sedimentation in the Arctic Ocean is strongly controlled by sea ice that acts as
118 sediment carrier, but can also suppress sediment deposition under thick and persistent
119 ice cover (Darby et al., 2006; Polyak et al., 2009). During glacial/deglacial events,
120 multiple icebergs discharged into the Arctic Ocean from the termini of marine-based
121 ice sheets and strongly affected sediment dispersal and deposition (e.g., Spielhagen et
122 al., 2004; Polyak et al., 2009). Fine-grained sediments can also be transported by
123 subsurface and deep-water currents, such as the Atlantic water (Winkler et al., 2002),
124 but their role in the overall Arctic Ocean sedimentation is not well understood.

125

126 **3. Materials and methods**

127 Gravity core ARC4-BN05 (referred hereafter as BN05) was collected from the
128 Canada Basin in the vicinity of the Mendeleev Ridge ($80^{\circ} 29.04' N$, $161^{\circ} 27.90'$
129 W , 3156 m water depth) (Fig. 1) on the fourth Chinese National Arctic Research
130 Expedition (CHINARE-IV) in 2009. The BN05 site was chosen in a close proximity
131 to earlier investigated cores FL224 and PS72/392-5 (Stein et al., 2010a) to enable



132 robust correlation with the established stratigraphies. A total of 119 samples were
133 taken at 2-cm intervals over the 238-cm BN05 length, and kept frozen until analyzed.

134 For age constraint within the radiocarbon range, Accelerator Mass
135 Spectrometry ^{14}C dating was performed on 1000–1200 tests of planktic foraminifers
136 *Neogloboquadrina pachyderma* sin. ($>63\ \mu\text{m}$) from core depths at 4-6, 8-10, 18-20
137 and 22-24 cm, using the NOSAMS facilities at Woods Hole Oceanographic
138 Institution.

139 For grain-size analysis, ~2-g sediment samples were successively treated with
140 15 ml 15% H_2O_2 , 5 ml 3mol/L HCl, and 20 ml 1mol/L Na_2CO_3 for removing organic
141 matter, biogenic carbonates, and biogenic silica, respectively. Grain size
142 measurements in the range of 0.02 to 2000 μm were performed on a Malvern
143 Mastersize laser particle sizer (Mastersizer 2000) in the First Institute of
144 Oceanography, SOA, China.

145 Coarse sediment $>63\ \mu\text{m}$ was sieved from ~10–15 g samples and counted under
146 the microscope for foraminiferal and mineral grain numbers.

147 Elemental abundances, given in peak area (counts per second, cps), were
148 obtained at 1 cm resolution using the Itrax XRF core scanner at the Polar Research
149 Institute of China, setting at 20 s count times, 10 kV X-ray voltage and an X-ray
150 current of 20 mA. The obtained count values are used as estimates of relative
151 concentrations. In addition, concentrations of major elements, such as Ca and Mn,
152 were determined on point samples by ICP-OES (iCAP6300) at the First Institute of
153 Oceanography, SOA, China, following the standard procedures.



154 Color reflectance was measured using a hand-held Minolta CM-2002
155 spectrofotometer at 1 cm intervals. Only the grayscale lightness index (L^*) is used in
156 this paper.

157 A total of 60 2-cm-thick samples were collected at 4-cm interval for
158 paleomagnetic measurements performed at the Paleomagnetism and Geochronology
159 Laboratory of the Institute of Geology and Geophysics, Chinese Academy of Science.
160 Magnetic susceptibility was measured using the KLY-4s Kappabridge instrument.
161 Subsequently, stepwise alternating field (AF) demagnetization of natural remanent
162 magnetization (NRM) was conducted using the 2-G Enterprises Model 760-R
163 cryogenic magnetometer (2G760) installed in a magnetically shielded (<300 nT)
164 space. AF demagnetization steps of 5-10 mT were used up to a maximum AF of 100
165 mT.

166 For bulk sediment mineralogy ~5-g samples were dried, pulverized, passed
167 through a 200 mesh sieve, and loaded into aluminum holders. Samples were X-rayed
168 from 5 to $65^\circ 2\theta$ with Cu K-alpha radiation (40 kV, 100 mA) using a step size of
169 $0.02^\circ 2\theta$ and a counting time of 2 s per step on a D/max-2500 diffractometer (XRD)
170 equipped with a graphite monochromator with 1° slits in the laboratory of the First
171 Institute of Oceanography, SOA, China. Prior to the analysis, instrument was blank
172 corrected and all samples were measured under the same conditions. Peak areas were
173 estimated from XRD traces using Jade6.0 software, and semi-quantitative estimates of
174 bulk mineral percentages were calculated following Cook (1975). The windows (2 θ),
175 range of spacings (λ) and intensity factors of minerals were determined based on



176 Cook (1975) are listed in Table 1.

177 Samples for clay minerals determination (~5g) were first treated with H₂O₂ (10%)
178 and HCl (1mol /L) to oxidize the organic matter and remove the carbonates,
179 respectively. Clay fractions (< 2 μm) were obtained by the Atterberg settling tubes
180 method according to Stoke's Law. Each sample was transferred to two slides by wet
181 smearing. Samples were then air-dried prior to XRD analysis. One sample slide was
182 air dried at 60 °C for 2 h and analyzed. The second sample was solvated with ethylene
183 glycol in an underpressured desiccator for at least 24 h at 60 °C. Every
184 ethylene-glycol solvated sample was measured twice: the first scanning was done
185 from 3° to 30° 2θ with a step size of 0.02°, and the second scanning from 24° to 26°
186 2θ with a 0.01° step. The latter was run as a slow scan to distinguish the 3.54/3.58 Å
187 kaolinite/chlorite double peak. Clay minerals were also identified by X-ray diffraction
188 (XRD) using a D/max-2500 diffractometer with CuKα radiation (40 kV and 100 mA)
189 in the laboratory of the First Institute of Oceanography, SOA, China. Peak areas
190 representing the clay mineral groups were estimated from glycolated XRD traces
191 using the 17 Å smectite, 10 Å illite, and 7 Å chlorite plus kaolinite peaks. Chlorite
192 (004) was identified at 3.54Å and kaolinite (002) at 3.58Å (Biscaye, 1964),
193 respectively. Semi-quantitative estimates of clay mineral percentages were calculated
194 by means of Biscaye's factors (1965).

195 To enhance the interpretation of downcore proxy distributions, Principal
196 Component Analysis (PCA) was performed in MATLAB [MathWorks, 2014]. PCA
197 included all analyzed mineralogical proxies along with main grain-size groups (clay,



198 silt, fine to medium sand (63-250 μ m), and coarser grains), Ca and Mn concentrations
199 (ICP-OES), and foraminiferal numbers.

200

201 **4. Results**

202 **4.1 General stratigraphy**

203 As common for sediment cores from the Arctic Ocean (e.g., Jakobsson et al.,
204 2000; Polyak et al., 2004, 2009; Spielhagen et al., 2004; Stein et al., 2010a, b), core
205 ARC4-BN05 displays distinct cycles in sediment color and composition expressed in
206 interlamination of dark brownish and lighter-colored grayish muds (silty clays, clay
207 silts and sandy silt), with coarser dropstones occurring in several layers. This color
208 cyclicity is approximated by changes in sediment lightness that largely mirrors the
209 content of Mn (Fig. 3), consistent with other studies from the Arctic Ocean (e.g.,
210 Jakobsson et al., 2000; Polyak et al., 2004; Adler et al., 2009). We identify 18
211 distinctly brown units, from B1 to B18, characterized by elevated content of Mn (Fig.
212 3). Another prominent lithostratigraphic feature in the western Arctic Ocean, widely
213 used for core correlation, is pink-white to whitish layers (PW) rich in detrital
214 carbonates (e.g., Clark et al., 1980; Polyak et al., 2009; Stein et al., 2010a, b). We
215 identify three major PW layers expressed both visually and in high Ca content (Fig.
216 3).

217 Foraminiferal abundances are generally high (mostly >50% of >63 μ m grains) in
218 brown units, except for B11-B13 and below B17-B18, and are very low to absent in



219 grey units. This pattern is consistent with foraminiferal stratigraphy reported in earlier
220 studies from the western Arctic Ocean (e.g., cores NP-26, HLY0503-JPC6 & 8,
221 P1-92AR-P23 & 39; Polyak et al., 2004, 2013; Adler et al., 2009; Cronin et al., 2013;
222 Lazar and Polyak, 2016).

223

224 **4.2 AMS ^{14}C dating**

225 The measured AMS ^{14}C ages of core ARC4-BN05 were calibrated to calendar
226 ages based on calibration using CALIB 7.10 (<http://calib.org/calib/calib.html>) (Table
227 2). The reservoir corrections of 790 and 1400 years were applied to Holocene and
228 glacial-age samples, respectively, according to Coulthard et al. (2010) and Hanslik et
229 al. (2010). Same corrections have also been applied to ^{14}C ages in core 03M03 from
230 the Chukchi Abyssal Plain (Fig. 2; Wang et al., 2013).

231

232 **4.3 Paleomagnetic stratigraphy**

233 While detailed paleomagnetic investigation is not an objective of this paper, we
234 utilize the inclination data for an independent stratigraphic constraint in line with
235 earlier studies (e.g., Jakobsson et al., 2000; Spielhagen et al., 2004; Polyak et al.,
236 2009). Paleomagnetic inclination in core ARC4-BN05 shows mostly positive values
237 oscillating around $+70^\circ$ in the upper part of the core, with a major polarity change
238 occurring at ~ 120 cm (Fig.3). A similar inclination drop has been identified in



239 multiple sediment cores across the Arctic Ocean in the same stratigraphic position
240 within estimated MIS 7, although the nature of this change in paleomagnetic
241 characteristics is not well understood (e.g., Jakobsson et al., 2000; Polyak et al., 2009;
242 Xuan and Channell, 2010).

243 Other paleomagnetic parameters, such as magnetic susceptibility (MS), can
244 provide additional correlation means (e.g., Sellén et al., 2010). Two prominent peaks
245 in MS occur in the intervals between units B7/B8 and B10/ B11 (Fig. 3).

246

247 **4.4 Grain size and dropstones**

248 Based on the results of grain-size analysis, sediment in core BN05 can be
249 generally classified as sandy mud, poorly to very poorly sorted, mostly coarse-skewed,
250 and strongly leptokurtic (peaked). Generally, silt and clay predominate grain-size
251 composition (33-60% and 23-61%, respectively), but coarser particles also make a
252 considerable contribution, with up to >30% peak contents of sand (>63 μ m) (Fig. 4a).
253 Coarse size fractions, from coarse silt to various sand fractions (e.g., >63, >125, and
254 >250 μ m) mostly co-vary downcore.

255 Grain size distribution is mostly polymodal with three distinct major modes
256 centered at ~4, 7-7.5, and 85-90 μ m, plus a smaller but consistent mode at ~400-450
257 μ m (Fig. 4b), which can be approximated by clay (<4 μ m), silt, and sand size
258 fractions. Mode 1 (4- μ m) is overall most common in core BN05, occurring mostly in
259 combination with the fine- and/or coarse-sand mode, but also forming very



260 fine-grained intervals (e.g., at 37 cm, Fig. 4b). Mode 2 (7-7.5 μm) is common in the
261 lower part of the core (below \sim 175 cm), where it mostly co-occurs with mode 1 and
262 coarse-grain tail, and also in distinct grey units around 30-40 and 90-100 cm in
263 combination with the fine-sand mode 3 (e.g., 39 and 93 cm, Fig. 4b).

264 Several core intervals contain large rock fragments >5 mm (dropstones). These
265 rock fragments are mostly poorly rounded, subangular to angular in shape.

266 Composition of sampled dropstones is illustrated in Fig. 4c. Most dropstones are
267 represented by dolomite and low metamorphic quartz sandstone fragments of up to 5
268 cm in diameter. Also found were individual dropstones composed of volcanic rock
269 and shale, as well as a few greisen dropstones near the base of the core.

270

271 **4.5 Sediment mineralogy**

272 The clay assemblage in samples from core ARC4-BN05 mainly consists of illite,
273 chlorite, kaolinite and smectite (Fig. 5). The illite group is overall the major
274 constituent of the clay mineral fraction, ranging between 43% and 73%. Its downcore
275 distribution pattern is opposite to that of the three other major clay-mineral groups -
276 kaolinite, chlorite, and smectite, which mostly co-vary except for some
277 lithostratigraphic intervals, such as PW layers. Elevated content of these clay minerals
278 is characteristic for grayish sedimentary units.

279 The bulk mineral assemblage in core ARC4-BN05 mainly consists of quartz,
280 K-feldspar, plagioclase, calcite, dolomite and pyroxene (Fig. 5). Quartz is generally



281 the most abundant mineral ranging between 20% and 51% and typically peaking in
282 grayish sediment units. K-feldspar, plagioclase and pyroxene (mainly augitic) mostly
283 co-vary, with peaks in grey units in the upper part of the core, but more in brown units
284 in the lower part starting from unit B10. Calcite has a high content in brown units of
285 the upper part and much lower values below unit B9. Dolomite distribution shows
286 distinct peaks reaching up to 53%, with the highest peaks occurring in the PW layers.
287 Similar to other minerals, the pattern of dolomite distribution changes around unit
288 B10, with maxima in thick grey units below and in thin interlayers within brown units
289 above this stratigraphic level.

290

291 **4.6 Principal Component Analysis**

292 The first three Principal Components identified by PCA with a Varimax rotation
293 account for 19%, 18%, and 17% of the total variance. This relatively low and evenly
294 distributed communality of the leading PCs reflects a complexity of multi-proxy
295 variables characterizing sedimentary environments and provenance, and their strong
296 variability occurring over multiple climatic cycles. Despite this variability, the PCs
297 identify several robust variable groups as shown in the PC loading score plots (Fig. 6).
298 Most of the groupings are well reproduced in PC1-2 and PC2-3 plots, with just a few
299 differences, such as a configuration of coarse grain-size fractions (high PC1 loading
300 score for silt vs. high PC3 score for fine sand).

301

302 **5. Discussion**



303 5.1 Stratigraphic framework

304 As no single existing chronostratigraphic method can comprehensively constrain
305 the age of the Arctic Ocean Pleistocene sediments, the age model for core
306 ARC4-BN05 was developed by correlating multiple proxies (such as paleomagnetic,
307 foraminiferal, and lithological) to earlier established Arctic Ocean stratigraphies (e.g.,
308 Adler et al., 2009; Polyak et al., 2009, 2013; Stein et al., 2010a), combined with ^{14}C
309 ages in the youngest part of the record (e.g., Fig. 7).

310 The two ^{14}C dates from the uppermost, 10-cm-thick brown sedimentary unit (B1)
311 in core ARC4-BN05 clearly identify its Holocene age (Table 2; Fig. 3). Compilations
312 of ^{14}C ages from the surficial and downcore sediments in the western Arctic Ocean
313 (Polyak et al., 2009; Xiao et al., 2014) indicate that the age of this unit extends from
314 ~2-3 ka on top to ~10-11 ka at the bottom contact, although an accurate estimate is
315 impeded by the uncertainties with the reservoir ages.

316 Two ^{14}C dates of ca. 42-44 ka from the brown unit B2 (Table 2; Fig. 3)
317 apparently fall into MIS 3, consistent with earlier stratigraphic results (e.g., Polyak et
318 al., 2004, 2009; Adler et al., 2009; Stein et al., 2010a). These ages should be, however,
319 considered as crude estimates as they are close to the ^{14}C dating limit, and the age
320 distribution in B2 has common inversions (e.g., Polyak et al., 2009). In cores with
321 relatively elevated sedimentation rates this unit occurs as two distinct brown layers,
322 indicated in some papers as B2a and B2b (e.g., Stein et al., 2010a, b; Wang et al.,
323 2013). In core ARC4-BN05 this partitioning is less apparent due to low sedimentation
324 rates, but the brownish sediment on top of the coarse detrital carbonate peak PW/W3,



325 typically located between B2a and B2b, probably corresponds to B2a.

326 An abrupt increase in sediment age between closely spaced B1 and B2 in core
327 ARC4-BN05 suggests a very condensed section or a hiatus between MIS 1 and MIS 3.
328 This age distribution is common for the western Arctic Ocean, and has been attributed
329 to very low to no sedimentation due to a very solid sea-ice cover or an ice shelf during
330 the Last Glacial Maximum in MIS 2 (e.g. Polyak et al., 2009; Wang et al., 2013).

331 Below the range of ^{14}C ages the age model is based entirely on proxy
332 correlations with earlier developed Arctic Ocean stratigraphies (e.g., Fig. 7). This
333 correlation is enabled by the cyclic nature of sediment lithology and attendant proxies,
334 where brown and grayish units generally correspond to interglacial (or major
335 interstadial) and glacial climatic intervals, respectively (e.g., Jakobsson et al., 2000;
336 Polyak et al., 2004, 2009; Adler et al., 2009; Stein et al., 2010a, b). In addition,
337 correlation tie points are provided by rare or unique events, such as prominent detrital
338 carbonate peaks (PW/W), major paleomagnetic inclination swings, and changes in
339 foraminiferal assemblages and abundance pattern.

340 According to this approach, we identify foraminiferal- and Mn-rich brown units
341 B3-B7 and B8-B10 as warm substages of MIS 5 and 7, respectively (Figs. 3, 7). This
342 age assignment is corroborated by the prominent detrital carbonate peaks PW2 and 1
343 near the bottom of MIS 5 and 7, respectively. Furthermore, the principal drop in
344 paleomagnetic inclination in core ARC4-BN05 occurs in the lower part of MIS 7,
345 consistent with many cores from the Arctic Ocean (e.g., Jakobsson et al., 2000;
346 Spielhagen et al., 2004; Adler et al., 2009; Polyak et al., 2009). Solidly grayish,



347 foraminiferal and Mn-poor unit separating brown units B2 and B3 is accordingly
348 considered as related to glacial MIS 4, and a similar unit between B7 and B8 – to MIS
349 6. It is possible, however, that most of the fine-grained, greyish sediment was
350 deposited during deglaciations following the actual glacial intervals, which may have
351 been very compressed, similar to the LGM.

352 Stratigraphy below MIS 7 has been less investigated in prior studies, and
353 therefore the age model for the lower part of the core is more tentative. Nevertheless,
354 a prominent oldest foraminiferal peak in units B14-B16 (Fig. 3) allows us to identify
355 these units as MIS 11 by comparison with other microfaunal records reported from
356 the western Arctic Ocean (e.g., Cronin et al., 2013; Polyak et al., 2013). MIS 13 and
357 15 have been tentatively assigned to Units B17 and B18 underlying a prominent grey
358 interval attributed to MIS 12. Overall, the record in core ARC4-BN05 is estimated to
359 represent the last ca. 0.5-0.6 Ma, that is, most of the middle to late Quaternary with an
360 average sedimentation rates of 4-5 mm/ka.

361

362 **5.2 Depositional environments and sediment provenance**

363 Distribution of various terrigenous components in Arctic sediment records
364 carries information on sediment sources and depositional environments, and thus
365 paleocirculation and changes in paleoclimatic conditions, such as connection to other
366 oceans and build-up/disintegration of ice sheets (e.g., Bischof and Darby, 1997;
367 Krylov et al., 2008; Polyak et al., 2009; Stein et al., 2010a, b; Yurco et al., 2010;



368 Fagel et al., 2014). We utilize the data on clay and bulk minerals along with the grain
369 size and total Ca and Mn distribution in core ARC4-BN05 to reconstruct changes in
370 glacial conditions and circulation in the western Arctic Ocean during several glacial
371 cycles extending to estimated ca. 0.5-0.6 Ma. In this work we capitalize on earlier
372 studies on the distribution of bulk and/or clay minerals in surface and downcore
373 Arctic Ocean sediments (e.g., Vogt, 1997; Stein, 2008; Krylov et al., 2014; Zou,
374 2016), corroborated by more targeted provenance proxies, such as radiogenic isotopes
375 (Bazhenova, 2012; Fagel et al., 2014), heavy minerals (Stein, 2008; Kaparulina et al.,
376 2015), composition of coarse debris (Bischof et al., 1996; Wang et al., 2013), and
377 iron-oxide grains (e.g., Bischof and Darby, 1997; Darby et al., 2002).

378

379 **5.2.1 Grain size and depositional processes**

380 A variable, mostly multimodal distribution of grain size in core BN05 indicates
381 multiple controls on sediment delivery and/or deposition. The prevailing mode 1 at ~4
382 μm , often in variable combinations with the fine-sand mode, is common for brown
383 units, except for the oldest layers (estimated MIS 13/15 and partly 11). This pattern is
384 similar to grain-size distribution with an average mode at ~3.4 μm reported for
385 Holocene sediments across the Arctic Ocean (Darby et al., 2009). Furthermore,
386 sediment in core BN05 with the same mode also makes up the most fine-grained
387 intervals in glacial/deglacial units, such as MIS 4 and 6 (Fig. 4b). We infer that mode
388 1 represents some combination of deposition from sea ice and from suspension that



389 could result from winnowing of fines from the basin margins and ridges during
390 interglacials, as well as overflow plumes discharged by retreating glaciers during
391 glacial/deglacial intervals. An occurrence of apparently similar grain-size pattern in
392 interglacial and fine-grained glacial/deglacial intervals might indicate a convergence
393 of glacial erosion processes with those related to sea-ice formation and transportation.
394 A similar grain-size interpretation has been earlier proposed for sediment from the
395 Canada Basin with the principal mode at $\sim 2 \mu\text{m}$ (Clark et al., 1980). This apparent
396 discrepancy may be related to the methodological offset between grain size
397 determined by the pipette method vs. laser diffraction, where the latter produces larger
398 diameters for fine sediment, especially in the presence of platy particles (Beuselinck
399 et al., 1998; Ramaswamy and Rao, 2006).

400 Mode 2 centered at $7\text{-}7.5 \mu\text{m}$ is more stratigraphically restricted. Its combination
401 with the fine-sand mode (e.g., Fig. 4b) is characteristic for coarser grained portions of
402 MIS 4, 6, and 12, which also have a specific mineralogical composition (PC loading
403 group 4: Fig. 6; Table 3). This distinct stratigraphic pattern suggests that the
404 formation of this sediment was related to glacial/deglacial processes; however, the
405 prevailing grain size mode around $7\text{-}7.5 \mu\text{m}$ is too coarse for suspension plumes and
406 too fine for massive deposition from icebergs. On the other hand, fine to medium silts,
407 susceptible to intermediate currents, are common for turbiditic deposits, including
408 glaciogenic environments (e.g., Wang and Hesse, 1996; Hesse and Khodabaksh, 2016).
409 We propose that mode 2 sediment type is related to glacial underflows that formed
410 debris lobes on glaciated margins grading into turbidites in the adjacent basins, along



411 with iceberg-rafted debris. Multiple debris lobes have been mapped on the Chukchi
412 and East-Siberian slopes in association with glaciogenic diamictons on the margin
413 (Jakobsson et al., 2008; Niessen et al., 2013; Dove et al., 2014). Close to the margins
414 glacioturbidites can form deposits of several meters thick (Polyak et al., 2007), but
415 thin out towards the inner parts of the basins, such as the BN05 site. In particular,
416 deposits similar to fine-grained turbidites, attributed to MIS 4/lower MIS 3, have been
417 recovered from the Northwind and Chukchi basins affected by glaciogenic inputs from
418 the Chukchi and East Siberian margins, respectively (Polyak et al., 2007; Matthiessen
419 et al., 2010; Wang et al., 2013). In the Chukchi Basin this unit, correlative to a much
420 thinner MIS 4 interval in core BN05, is characterized by a high content of fine silt
421 with a peaky downcore distribution (Wang et al., 2010, 2013).

422 Additionally, modes 1 and 2 make up a bimodal distribution in the lowermost
423 part of the core – mostly in estimated MIS 13/15 and near the bottom of MIS 11. The
424 predominant stratigraphic position in brown units makes unlikely the glaciogenic origin
425 of this sediment. We hypothesize that this grain-size pattern reflects a combination of
426 “normal” interglacial environments with winnowed silts deposited by downwelling of
427 shelf waters enriched in dense brines. Although no observational evidence exists for
428 such waters penetrating deeper than the halocline (~200 m) under modern Arctic
429 conditions, periods of stronger cascading in the past have been inferred from sediment
430 distribution on the slopes (Darby et al., 2009) and some sedimentary proxies, such as
431 radiogenic isotopes (Haley and Polyak, 2013; Jang et al., 2013). The bimodal
432 distribution of fine sediment in the lower part of the record is accompanied in most



433 samples by a small but consistent coarse-sand mode (400-450 μm), likely indicating
434 the presence of iceberg rafting.

435 Coarse sediment, up to dropstones of several cm large, is a consistent feature in
436 core BN05. In the apparent absence of strong current control on sedimentation, except
437 for some shelf areas, and a pervasive presence of floating ice, coarse sediment in the
438 Arctic Ocean is typically attributed to ice rafting, including sea ice and icebergs (e.g.,
439 Stein, 2008; Polyak et al., 2010, and references therein). Sedimentological studies in
440 areas of sea-ice formation or melting and in ice itself indicate that sediment carried by
441 sea ice in the Arctic Ocean is predominated by silt and clay, while coarser fractions
442 are of minor importance (Clark and Hanson, 1983; Nürnberg et al., 1994; Hebbeln,
443 2000; Darby, 2003; Dethleff, 2005; Darby et al., 2009). Some studies suggest a higher
444 content of sand in ice formed at the sea floor (anchor ice) (Darby et al., 2011), but the
445 contribution of this source yet needs to be evaluated. Furthermore, the role of sea ice
446 on sedimentation in the Arctic Ocean is not clear for glacial intervals, when most of
447 the sediment entrainment areas were exposed or covered by ice sheets. In contrast, in
448 iceberg-rafted sediment, deposited mostly in glacial/deglacial environments, the
449 content of large size fractions, from sand to boulders, is typically high, in excess of
450 10-20% (Clark and Hanson, 1983; Dowdeswell et al., 1994; Andrews, 2000). Thus,
451 elevated content of coarse sediment can be regarded as a good indicator of intense
452 iceberg rafting. Such events are not probable during full interglacials, exemplified by
453 modern conditions, but most likely occurred at times of instability and disintegration
454 of ice sheets that extended to the Arctic Ocean in the past (e.g., Spielhagen et al.,



455 2004; Stokes et al., 2005; Polyak et al., 2009).

456 In core BN05, coarse fractions (from coarse silt to sand) measured at different
457 sizes show very similar distribution patterns (Fig. 4a), indicating the same
458 predominant delivery mechanism, that is, iceberg rafting. This pattern is reflected in a
459 good correlation of fine to medium sand (63-250 μm) with coarser, $>250\mu\text{m}$ fractions,
460 that defines one of the PC loading groups (Fig. 6, Table 3). Increased coarse-grain
461 content mostly characterizes grayish units, especially near gray-to-brown sediment
462 transitions, and the PW layers, but also occurs in brown units in the upper part of the
463 record. The latter peaks enriched in detrital carbonates (high dolomite and total Ca)
464 represent interstadial or incomplete interglacial conditions, such as MIS 3, MIS 5a,
465 and parts of MIS 7.

466 A common occurrence (separate or combined) of two coarse grain modes,
467 around 85-90 and 400-450 μm , may indicate different sources for iceberg-rafted
468 material or different thresholds for glacial disintegration of various rock types. While
469 a more thorough interpretation requires further research, we note that grain-size mode
470 1 may co-occur with both fine-and coarse-sand modes, mode 2 – only with the
471 fine-sand mode, and bimodal 1/2 sediment type – only with the coarse-sand one.

472

473 **5.2.2 North American provenance**

474 One of the most robust PC loading groups is distinctly characterized by high
475 loadings of dolomite, total Ca content, and quartz/feldspar index (Group 2: Fig. 6,



476 Table 3). Dolomite is known as a robust indicator of the North American provenance
477 in the western Arctic, especially in relation to glacial inputs (e.g., Vogt, 1997; Zou,
478 2016). Dolomite is the main contributor of total Ca in sediment cores from the
479 western Arctic Ocean, with an especially high content in multiple coarse-grain peaks
480 (Bischof et al., 1996; Phillips and Grantz, 2001; Polyak et al., 2009; Stein et al., 2010a,
481 b). This dolomite is related to the extensive, carbonate-rich Paleozoic terrane in the
482 northern Canada (North American Platform; Fig. 1) that has been repeatedly eroded
483 during the Pleistocene by the LIS. The distribution of dolomite in Arctic sediment
484 cores can thus be used for reconstructing the history of the LIS sedimentary inputs.

485 Consistent with dolomite distribution in many other cores from the western
486 Arctic Ocean, its overall high content in core ARC4-BN05 has major peaks
487 corresponding to visually identifiable PW/W layers enriched in coarse debris (Fig. 5).
488 As has been suggested in earlier studies (e.g., Stokes et al., 2005; Polyak et al., 2009),
489 we infer that the dolomite peaks are related to pulses of massive iceberg discharge
490 from the LIS during the periods of its destabilization and disintegration. Furthermore,
491 radiogenic isotope studies demonstrate that fine sediment in the dolomitic peaks also
492 has North American provenance (Bazhenova, 2012; Fagel et al., 2014). These results
493 indicate that dolomite may have been transported not only by icebergs, but also in
494 meltwater plumes coming during deglaciations from the Canadian Archipelago or the
495 Mackenzie River.

496 As noted above, a change in the stratigraphic pattern of dolomite distribution
497 occurs around unit B10 estimated to correspond to the lower part of MIS 7 (Fig. 5). In



498 older sediments dolomite maxima co-occur with glacial (predominantly gray)
499 intervals, whereas, in the younger stratigraphy dolomite peaks in brown sediment or
500 grayish interlayers within brown units (MIS 3, 5, and 7), presumably corresponding to
501 transitional paleoclimatic environments, such as interstadials or stadials within
502 complex interglacial stages.

503 Another mineral indicator related to the North American provenance is a
504 quartz/feldspar ratio due to a considerable presence of sedimentary rocks enriched in
505 quartz, but not feldspar, in the Canadian Arctic in comparison with the Siberian
506 margin (e.g., Vogt, 1997; Zou, 2016; Kobayashi et al., 2016). In core ARC4-BN05
507 the distribution of this index is generally similar to dolomite, except for some peak
508 intervals, notably low Qz/Fsp values in PW1 and 3 (Fig. 6).

509

510 **5.2.3 Siberian provenance**

511 Mineral proxies potentially linked to Siberian provenance make two distinct
512 groups, as reflected in the PCA results (Groups 3 and 4: Fig. 6, Table 3). Group 3
513 comprises primarily pyroxene, feldspar, and plagioclase, and strongly anticorrelates
514 with the North-American proxies, such as Qz/Fsp and dolomite. The downcore
515 distribution pattern of this group changes from the affinity to interglacials in the lower
516 part of the record to peaks in glacial/deglacial intervals related to MIS 4 and 6. The
517 major source for pyroxene in the Arctic Ocean is the Siberian trap basaltic province
518 that drains to the Kara Sea and western Laptev Sea (Fig. 1; Washner et al., 1999;



519 Schoster et al., 2000; Krylov et al., 2008). On the other hand, basaltic rocks related to
520 the Okhotsk-Chukotka province (Fig. 1) may have also provided a significant source of
521 pyroxenes, as exemplified in surface sediments by a relative pyroxene enrichment in
522 the Chukchi Basin on the background of overall low values in the western Arctic Ocean
523 (Dong et al., 2014). Distributions of feldspar and plagioclase at the Siberian margin
524 show elevated contents occurring both in the western Laptev Sea and the East
525 Siberian Sea (Zou, 2016).

526 Based on a considerable affinity of the pyroxene-feldspar group to brown units
527 and a lack of correlation with coarse sediment fractions, we infer that it is primarily
528 related to sea-ice transport during interglacial/deglacial intervals, with sources
529 potentially including the East Siberian margin and more westerly areas. The
530 difference in both the sources and delivery processes from the LIS proxies may
531 explain an especially strong opposition of these groups. Multiple studies suggest that
532 sea ice from the Kara and Laptev seas may transport sediments to the Canada Basin
533 under favorable atmospheric conditions, such as the positive phase of the Arctic
534 Oscillation (Behrends, 1999; Darby et al., 2003; Darby et al., 2004; Yurco et al., 2010;
535 Darby et al., 2012), although it remains to be investigated, to what extent this
536 circulation pattern could have provided a significant sediment source for the western
537 Arctic Ocean in the Pleistocene.

538



539 **5.2.4 East-Siberian Ice Sheet**

540 The other group with a potentially Siberian provenance (Group 4: Fig. 6, Table 3)
541 comprises clay minerals smectite, kaolinite, and chlorite, and is related to overall
542 coarse sediment, especially consistently to fine sand (63-250 μm). This composition is
543 especially characteristic for intervals estimated as MIS 4, 6, and 12. The association
544 of clay minerals with coarse sediment is unusual and suggests that they may have
545 been derived by glacial erosion of source hard rocks. This linkage has been elaborated
546 for kaolinite distribution in the Barents Sea and central Arctic Ocean (Junttila, 2007;
547 Vogt and Knies, 2009; Krylov et al., 2014). While kaolinite sources, such as
548 Meso-Cenozoic paleosols and shales, are mostly known in the western Arctic from
549 northern Alaska and Canada (Naidu et al., 1971; Darby, 1975; Dalrymple and Maass,
550 1987), kaolinite weathering crusts have been also described from the East Siberian
551 margin (Slobodin et al, 1990; Kim and Slobodin, 1991). Smectite, which is typically
552 related to chemical weathering of basic rocks has been mostly associated in Arctic
553 sediments with delivery from Siberian trap basalts (Fig. 1) as reflected in the surface
554 sediments, suspended particulate material, and sea-ice samples from the Kara Sea and
555 western Laptev Sea (Stein et al., 1994; Wahsner et al., 1999; Schoster et al., 2000;
556 Dethleff et al., 2000). Peaks of smectite related to that source are especially
557 characteristic for deglacial intervals in sediment cores from the eastern Arctic Ocean
558 (Vogt and Knies, 2008). However, considerable sources of smectite also exist further
559 east along the Siberian margin due to basaltic outcrops related to the
560 Okhotsk-Chukotka volcanic province (Fig. 1), resulting in high content of smectite in



561 surface sediments of the East Siberian and Chukchi seas (Naidu et al., 1982;
562 Viscosi-Shirley et al., 2003; Nwaodua et al., 2014). Chlorite is also common in
563 surface sediments and suspended particulate material at the East Siberian margin
564 (Dethleff et al., 2000; Viscosi-Shirley et al., 2003). Modern and Holocene sediments
565 on the Chukchi shelf are especially enriched in chlorite due to advection from the
566 North Pacific at high sea-level stands (Kalinenko, 2001; Ortiz et al., 2009; Nwaodua
567 et al., 2014; Kobayashi et al., 2016), however this mechanism is only applicable to
568 interglacial periods.

569 We infer that sediment with a concerted enrichment in smectite, kaolinite, and
570 chlorite clay minerals associated with coarse fractions was transported to the Canada
571 Basin primarily in relation to the existence of large ice sheets in northern East Siberia
572 during glacial periods. Radiogenic isotope signature in upper Quaternary records from
573 the Mendeleev Ridge also indicates that the Okhotsk-Chukotka volcanic rocks
574 provided one of the principal end members, especially during MIS 4 and 6
575 (Bazhenova, 2012; Fagel et al., 2014). This sediment had to be transported into the
576 Arctic Ocean directly from the East-Siberian/Chukchi margin as the alternative
577 pathway via the Bering Sea only operated at high interglacial sea levels, when the
578 Bering Strait was open for throughflow (e.g., Keigwin et al., 2006; Ortiz et al., 2009).
579 Considering an affinity of the kaolinite-smectite-chlorite group with sediments
580 coarser than clays, corresponding to grain-size modes 2 and 3, their distribution across
581 the basin was likely related to iceberg rafting and glacial underflows, as discussed
582 above in section 5.2.1. A relatively fast and direct delivery mechanism by debris



583 flows and ensuing turbidites may explain a good preservation of fragile clay minerals,
584 normally not resistant to physical erosion.

585 Some early paleoglaciological studies proposed the existence of a thick
586 Pleistocene ice sheet centered over the East Siberian shelf (Hughes et al., 1977;
587 Grosswald and Hughes, 2002). The inference of former ice sheets/shelves in this
588 region is now corroborated by multibeam bathymetry and sub-bottom data revealing
589 multiple glacial features on the top and slopes of the Chukchi and East Siberian
590 margin (Polyak et al., 2001, 2007; Jakobsson et al., 2008, 2014, 2016; Niessen et al.,
591 2013; Dove et al., 2014). ESIS has also been reproduced by numerical paleoclimatic
592 modeling for a large Pleistocene glaciation exemplified by MIS 6 (Colleoni et al.,
593 2016). Sedimentary proxies indicative of the Okhotsk-Chukotka provenance in cores
594 from the Canada Basin provide an additional tool for reconstructing the ESIS history.
595

596 **5.2.5 Interglacial signature**

597 Data points from brown units make up a distinct PC loading group with Mn,
598 foraminiferal numbers, and fine sediment as lead variables (Group 1: Fig. 6; Table 3).
599 This composition is consistent with the modern-type Arctic Ocean environments
600 characterized by predominant controls of sediment deposition by sea ice, considerable
601 biological activity in summer, and high sea levels. The latter is important for
602 providing supply of Mn from the surrounding shelves (März et al., 2011; Löwemark
603 et al., 2014). The same condition may also control biological production, and thus



604 foraminiferal numbers, via export of nutrients from the marginal seas (e.g., Xiao et al.,
605 2014), although interaction of this factor with sea-ice conditions yet needs to be
606 clarified.

607 The two minerals having the closest distribution to PC loading group 1,
608 consistent with a predominant occurrence in brown, interglacial/major interstadial
609 units, are illite and calcite (Figs. 5, 6). Illite is a typical high-latitude clay mineral,
610 mainly supplied by physical weathering of metasedimentary and plutonic rocks
611 (Chamley, 1989; Junttila, 2007). High illite concentrations in surficial Arctic Ocean
612 sediments have been found in many areas including the Alaska margin and adjacent
613 Canada basin (Dong et al., 2014; Kobayashi et al., 2016), East Siberian Sea and the
614 adjacent part of the Laptev Sea (Wahsner et al., 1999; Kalinenko, 2001; Viscosi-
615 Shirley et al., 2003; Dethleff, 2005; Zou., 2016), and northern Greenland and
616 Svalbard regions (Stein et al., 1994). In core ARC4-BN05 illite has consistently high
617 values in generally fine-grained brown units (Fig. 5), although peak values may not
618 exactly coincide with those of Mn or foraminiferal numbers. In addition, illite shows a
619 prominent peak in a very fine-grained interval at ~35 cm within glacial/deglacial
620 sediment of estimated MIS 4. This distribution is consistent with the pattern in both
621 surface sediments and sediment cores, where illite is characteristic for fine-grained
622 sediment indicative of transportation by sea ice or in the water column (Krylov, 2014).
623 As shown by sediment-core studies, these mechanisms can provide high illite levels
624 under both interglacial (this study) and glacial/deglacial environments (Knies and
625 Vogt, 2003; Yurco et al., 2010). The latter is probably associated with deposition of



626 fine sediment from glacial overflows, as exemplified by the fine-grained part of MIS
627 4 deglaciation.

628 High contents of calcite in core ARC4-BN05 co-occur with high numbers of
629 foraminifers (Figs. 3 and 6), indicating that calcite in these sediments is to a large
630 extent biogenic, consistent with earlier results from the study area (Stein et al., 2010a).
631 Nevertheless, in the lower part of the record, where calcareous fossils are mostly not
632 preserved, calcite shows a considerable affinity to dolomite, which corroborates a
633 mixed, biogenic and detrital nature of calcite in Arctic Ocean sediments (e.g., Vogt,
634 1997).

635

636 **5.3 Evolution of sedimentary environments**

637 **5.3.1 PC scores in the stratigraphic context**

638 The stratigraphically changing pattern of sediment delivery and deposition,
639 including cyclic glacial-interglacial fluctuations and longer-term changes, indicates
640 complex interactions of climatic and oceanographic factors controlling depositional
641 environments. To gain more insight into these changes, we plotted the distribution of
642 PC scores grouped by individual glacial and interglacial stages, along with the PC
643 loading interpretation (Fig. 8).

644 A long-term trend in interglacial environments is indicated by a shift from (1)
645 predominantly Siberian to more North American provenance, especially strong in
646 MIS 5 and 1, and (2) from negative to increasingly positive scores of interglacial



647 proxies with a threshold around the bottom of MIS 7 (Fig. 8a). Glacial environments
648 show an apparently more complex provenance change, with Siberian sources
649 predominating early and late glacial stages (MIS 12-14 and MIS 4-6, respectively)
650 and Laurentide provenance controlling MIS 8 and 10 (Fig. 8b). In addition,
651 interglacial positive signature characterizes some intervals in MIS 4 and 6 as well as
652 intermittent (stadial) intra-MIS 3, 5, and 7 events. We note that MIS 2 is not
653 represented in this data due to its very compressed nature.

654

655 **5.3.1 Glacial environments**

656 The identified changes in sedimentary environments and provenance can be
657 explained by several types of controls, including configuration of ice sheets against
658 sea level and climatic conditions, sediment delivery mechanisms, and circulation. Ice
659 sheet sites and geometry at specific time intervals dictate the timing and location of
660 major sediment discharge events into the Arctic Ocean. Transportation mechanisms,
661 such as by icebergs, debris flows, or suspension plumes, further control sediment
662 delivery to specific sites. Finally, oceanic circulation affects the distribution of
663 sediment across the oceanic basins. This may include surface circulation driving sea
664 ice, icebergs, and surface plumes, deep circulation affecting turbidite/contourite
665 pathways, and downwelling of sediment-laden dense waters.

666 We infer that sedimentary variations observed in core BN05 and correlative
667 records from the western Arctic Ocean can be explained by the evolution of



668 surrounding ice sheets and associated changes in oceanic conditions, such as
669 circulation, sea ice, and biota. It has been known from early studies (e.g., Clark et al.,
670 1980; Winter et al., 1997) that glacial, notably LIS impact on the western Arctic
671 Ocean has been steadily increasing over the time span covered by sediment cores
672 from this region. A recent investigation utilizing a more up-to-date stratigraphic
673 paradigm estimated the timing of a step increase in LIS inputs as ca. 0.8 Ma (Polyak
674 et al., 2013), consistent with the onset of major glaciations in the Northern
675 Hemisphere (Head and Gibbard, 2015). Core BN05 provides a record of sediment
676 deposition in the Canada Basin, and thus glacial inputs into the western Arctic Ocean
677 during most of the time interval to follow.

678 Considering the overall gradual growth of Pleistocene Arctic ice sheets, we infer
679 that the shift from Siberian to North American sources between MIS 12 and 10 was
680 primarily related to the expansion of the LIS, especially the northwestern Keewatin
681 sector that discharges into the western Arctic Ocean. However, its further growth may
682 have had an opposite effect due to a more massive ice sheet that required warmer
683 climatic conditions and/or higher sea levels to destabilize it. Based on data for the last
684 glacial cycle, the Keewatin sector of the LIS rested mostly on relatively elevated
685 terrane of the Canadian Archipelago and adjacent mainland, fringed by a narrow
686 continental shelf and dissected by numerous channels providing conduits for ice
687 streams and evacuation of icebergs at rising sea levels (Stokes et al., 2005, 2009;
688 England et al., 2009; Margold et al., 2015). The latter events are illustrated in BN05
689 data by intra-MIS 5 stadials with a consistent LIS signature (Fig. 8b). Especially high



690 LIS scores characterize PW layers 2 and 3 attributed to MIS 5d and late MIS 3,
691 respectively. A similar, LIS-dominated pattern likely represents the last deglaciation as
692 indicated by a number of provenance studies (e.g., Stokes et al., 2005; Bazhenova,
693 2012; Jang et al., 2013).

694 In comparison to the LIS, a presumably much smaller ESIS, formed on a broad
695 and overall flat East-Siberian/Chukchi margin (Niessen et al., 2013; Dove et al., 2014;
696 Colleoni et al., 2016), had to be responsive to sea-level changes even at low levels. It
697 may be possible that the ESIS also increased in size by MIS 6, known as a time of a
698 dramatic increase of glacial inputs from the Barents-Kara Ice Sheet into the eastern
699 Arctic Ocean (e.g., O'Regan et al., 2008). A synchronous MIS 6 expansion of both
700 North American and Siberian ice sheets and related ice shelves might explain the
701 deep-keel glacial erosion of the Lomonosov Ridge at modern water depths exceeding
702 1000 m (Jakobsson et al., 2016, and references therein).

703 A concurrent interpretation can be proposed with a focus on sediment
704 transportation processes as deposits of some glacial intervals, notably MIS 12 and
705 parts of MIS 4 and 6, are associated with grain size mode 2 potentially indicating
706 glacial debris flow/turbidite emplacement. Large debris flows entering the Chukchi
707 Basin and continuing as turbidites into Canada Basin, as exemplified by subbottom
708 sonar profiles (Niessen et al., 2013; Dove et al., 2014), may have overprinted
709 deposition from icebergs. We note that deposits of MIS 4 and 6 also contain intervals,
710 where Siberian provenance is combined with interglacial positive scores (Fig. 8b) due
711 to their fine-grained composition along with high illite content. These sediments



712 likely represent deposition from suspension plumes, potentially marking especially
713 strong deglacial meltwater discharge. A prominent fine grained, finely laminated
714 interval within MIS 4 deglaciation (possibly extending into MIS 3) has been reported
715 from multiple cores across the Chukchi Basin – Mendeleev Ridge area (Adler et al.,
716 2009; Matthiessen et al., 2010; Bazhenova, 2012; Wang et al., 2013).

717 Under modern conditions the BN05 site is mostly controlled by the Beaufort
718 Gyre current circulation system, although can also be affected by the Transpolar Drift
719 during strong shifts in the Arctic Oscillation (Rigor et al., 2002). This setting
720 probably applies to the Holocene and comparable interglacial conditions (Darby and
721 Bischof, 2004). Some authors suggested that during glacial periods the surface
722 circulation that controls pathways of iceberg and sea-ice drift may have been
723 considerably different from the modern pattern, with both North American and
724 Siberian sources shortcutting the Arctic Ocean towards the Fram Strait (Bischof and
725 Darby, 1997; Stärrz et al., 2012). These changes would have potentially affected the
726 study area, possibly making it more exposed to the Siberian provenance than under
727 present conditions. However, the existing reconstructions based on very limited
728 records with only crude stratigraphic controls, need to be elaborated by spatially and
729 stratigraphically more representative data constraining past circulation changes. In
730 particular, glacial maxima may be elusive, especially in the western Arctic Ocean, due
731 to extremely low sedimentation rates or a hiatus, as exemplified by the Last Glacial
732 Maximum (Polyak et al., 2009; Poirier et al., 2012).

733 An overall integration of potential controls on sediment deposition in the study



734 area during major identified types of glacial environments are illustrated in Fig. 9.
735 More studies are needed to discriminate between different controls, including proxy
736 records providing higher resolution for target intervals as well as modeling
737 experiments to test spatial and stratigraphic variability in such factors as iceberg and
738 meltwater discharge and their ensuing distribution pathways.

739

740 **5.3.2 Interglacial environments**

741 The long-term trend in interglacial environments reflected in a shift from
742 negative to increasingly positive scores of interglacial proxies with a threshold around
743 the bottom of MIS 7 (Fig. 8a) can be partially explained by the absence of calcareous
744 foraminifers in the lower part of the record. However, even MIS 11 that has abundant
745 foraminifers is in the interglacial negative domain, suggesting more controls. One
746 possibility is that this trend was related to the evolution of circum-Arctic ice sheets
747 that would have inevitable incurred changes in oceanic conditions, such as circulation
748 and sea ice. An expansion of perennial sea ice in the western Arctic Ocean near the
749 MIS 7 bottom has been proposed based on foraminiferal assemblages (Polyak et al.,
750 2013; Lazar and Polyak, 2016). This step change has been tentatively attributed to the
751 LIS growth that may have affected sea-ice conditions via increased albedo and/or
752 higher meltwater inputs. This inference is consistent with a change from Siberian to
753 North American provenance during interglacials in BN05 (Fig. 8a). In addition to a
754 more lingering LIS during interstadials/interglacials, this shift in provenance could be



755 related to a strengthening of the Beaufort Gyre as more sea ice filled the western
756 Arctic Ocean.

757 More limited sea-ice cover in the older part of the middle Pleistocene could have
758 also enhanced the production of dense brines at the Siberian margin, resulting in a
759 deeper convection and cascading of shelf sediments to the deep basin. This scenario
760 would explain an unusual grain-size composition of sediments in the older
761 interglacials combining mode 2, indicative of winnowed silt, with a typical
762 interglacial fine-grained mode 1.

763

764 **6. Summary and conclusions**

765 Sediment core ARC4–BN05 was collected from the Canada Basin in the vicinity
766 of the Chukchi Plateau and the Mendeleev Ridge, Arctic Ocean, on the fourth Chinese
767 National Arctic Research Expedition (CHINARE-IV). Based on correlation to earlier
768 proposed Arctic Ocean stratigraphies (e.g., Adler et al., 2009; Stein et al., 2010a;
769 Polyak et al., 2013) and AMS ¹⁴C dating of the youngest sediments, the BN05 record
770 covers the late to middle Quaternary (MIS 1-15, ca. 0.5-0.6 Ma). The core was
771 investigated for multiple sedimentary proxies including clay and bulk mineralogy,
772 grain size, paleomagnetism, elemental content, and planktonic foraminiferal numbers
773 with an average estimated age resolution of 4-5 ka per sample. This study, facilitated
774 by Principal Component Analysis of major paleoceanographic variables, provides
775 important new information about sedimentary environments and provenance in the



776 western Arctic Ocean on glacial time scales. The results enhance our knowledge on
777 the history of Arctic glaciations and interglacial conditions.

778 Glacially derived sediment can be discriminated between the North American
779 and Siberian provenance by their mineralogical and textural signature. In particular,
780 peaks of dolomite debris, including large dropstones, track the Laurentide Ice Sheet
781 (LIS) discharge events, while the East Siberian Ice Sheet (ESIS) inputs are inferred
782 from combined peaks of smectite, kaolinite, and chlorite associated with coarse
783 sediment. Siberian provenance is also identified from high content of pyroxene,
784 feldspar, and plagioclase, unrelated to coarse sediment. This sedimentary signature is
785 interpreted to indicate sea-ice transport from the Siberian margin during
786 interglacial/deglacial intervals. Full interglacial environments are characterized by
787 overall fine grain size, high content of Mn (and resulting dark brown sediment color),
788 and elevated contents of calcite and chlorite. Foraminiferal tests are abundant in
789 interglacial units in the upper part of the record (MIS 1-7) and estimated MIS 11, but
790 have very low numbers in other interglacials older than MIS 7, apparently due to
791 dissolution.

792 In addition to glacial-interglacial cyclicality, the investigated record indicates
793 variable impacts of LIS vs. ESIS on sediment inputs at different glacial events, along
794 with a long-term change in middle to late Quaternary sedimentary environments.
795 Based on the age model employed, major LIS inputs to the study area occurred during
796 MIS 3, intra-MIS 5 and 7 events, MIS 8, and MIS 10, while ESIS signature is
797 characteristic for MIS 4, MIS 6 and MIS 12. These differences may be related to



798 ice-sheet configurations at different sea levels, sediment delivery mechanisms
799 (iceberg rafting, suspension plumes, and debris flows), and surface circulation. A
800 long-term shift in the pattern of sediment inputs shows an apparent step change near
801 the estimated MIS 7/8 boundary (ca. 0.25 Ma), consistent with more sea-ice growth in
802 the Arctic Ocean inferred from benthic foraminiferal assemblages (Lazar and Polyak,
803 2016). This development of Arctic Ocean paleoenvironments possibly indicates an
804 overall glacial expansion at the western Arctic margins, especially in North America.
805 Such expansion may have affected not only glacial, but also interglacial conditions
806 via increased albedo and/or higher meltwater inputs, as well as a strengthening of the
807 Beaufort Gyre circulation as more sea ice filled the western Arctic Ocean.

808

809 **Acknowledgements**

810 We are grateful to the term of the Chinese fourth Arctic scientific expedition for
811 their assistance with sample collection. Special thanks are extended to Dr. Shijuan
812 Yan for the help with sampling and to Dr. Quanshu Yan for the help in editing of the
813 paper. This work was jointly supported by the Research Foundation of the First
814 Institute of Oceanography, State Oceanic Administration of China (No. 2013G07,
815 2014G30), the Chinese Special Project of Arctic Ocean Marine Geology Investigation
816 (No. CHINARE 2016-03-02), and the National Natural Science Foundation of China
817 (No. 41306205, 41676053, 40176136).

818



819 References

- 820 [1] Adler, R. E., Polyak, L., Ortiz, J. D., Kaufman, D. S., Channell, J. E.T., Xuan, C., Grottoli, A. G., Sellén,
821 E., Crawford, K. A.: Sediment record from the western Arctic Ocean with an improved Late Quaternary
822 age resolution: HOTRAX core HLY0503-8JPC, Mendeleev Ridge, **Global and Planetary Change**,
823 68,18-29,2009.
- 824 [2] Andrews, J. T.: Icebergs and iceberg rafted detritus (IRD) in the North Atlantic: Facts and assumptions,
825 **Oceanography**, 13(3), 100–108, 2000.
- 826 [3] Basilyan, A.E., Nikol'skiy, P.A., Maksimov, F.E., Kuznetsov, V.Y.: Age of Cover Glaciation of the New
827 Siberian Islands Based on ²³⁰Th/U-dating of Mollusk Shells, **Structure and Development of the**
828 **Lithosphere**, Paulsen, Moscow, pp. 506-514, 2010.
- 829 [4] Bazhenova, E.: Reconstruction of late Quaternary sedimentary environments at the southern Mendeleev
830 Ridge (Arctic Ocean), **PhD Thesis**, University of Bremen, Bremen, 83 p, 2012.
- 831 [5] Behrends, M.: Reconstruction of sea-ice drift and terrigenous sediment supply in the Late Quaternary:
832 heavy-mineral associations in sediments of the Laptev-Sea continental margin and the central Arctic
833 Ocean, **Reports on Polar Research**, 310, 1-167, 1999.
- 834 [6] Beuselink, L., Govers, G., Poesen, J., Degraer, G., Froyen, L.: Grain-size analysis by laser diffractometry:
835 comparison with the sieve-pipette method, **Catena**, 32, 193–208, 1998.
- 836 [7] Bischof, J. F. and Darby, D. A.: Mid-to Late Pleistocene ice drift in the Western Arctic Ocean: evidence
837 for a different circulation in the past, **Science**, 277, 74–78, 1997.
- 838 [8] Bischof, J.F., Clark, D.L., Vincent, J.S.: Origin of ice-rafted debris: Pleistocene paleoceanography in the
839 western Arctic Ocean, **Paleoceanography**, 11, 743–756, 1996.
- 840 [9] Biscaye, P.F.: Distinction between kaolinite and chlorite in recent sediments by X-ray diffraction,
841 **American Mineralogist**, 49, 1281–1289, 1964.
- 842 [10] Biscaye, P.F.: Mineralogy and sedimentation of recent deep-sea clay in the Atlantic Ocean and adjacent
843 seas and oceans, **The Geological Society America Bulletin**, 76, 803–832, 1965.
- 844 [11] Chamley, H.: Clay Sedimentology, **Springer**, Berlin. 623 pp, 1989.
- 845 [12] Clark, D. L., Whitman, R. R., Morgan, K. A., Mackey, S. D.: Stratigraphy and glacialmarine sediments
846 of the Amerasian Basin, central Arctic Ocean, **Geological Society of America**, Special Paper, 181, 57,
847 1980.



- 848 [13] Clark, D. and Hanson, A.: Central Arctic Ocean sediment texture: a key to ice transport mechanisms. **In:**
849 **Molnia, B.F. (Ed.), Glacial-Marine Sedimentation, Plenum Press**, New York, pp. 301–330, 1983.
- 850 [14] Clark, D. L., Chern, L. A., Hogler, J. A., Mennicke, C. M., Atkins, E. D.: Late Neogene climate evolution
851 of the central Arctic Ocean, **Marine Geology**, 93, 69–94, 1990.
- 852 [15] Colleoni, F., Kirchner, N., Niessen, F., Quiquet, A., Liakka, J.: An East Siberian ice shelf during the Late
853 Pleistocene glaciations: Numerical reconstructions, **Quaternary Science Reviews**, xxx, 1–16, 2016.
- 854 [16] Cook, H. E., Johnson, P.D., Matti, J.C., Zemmels, I.: Methods of sample preparation and X- ray
855 diffraction data analysis, X-ray mineralogy laboratory, **In: Kaneps AG**, ed. Init Repts, DSDP XXVIII,
856 999 -1007, [http://www.deepseadrilling.Org/28/volume/dsdp28- appendix-IV. Pdf](http://www.deepseadrilling.Org/28/volume/dsdp28-appendix-IV.Pdf), 1975.
- 857 [17] Coulthard, R.D., Furze, M.F.A., Pienkowski, A.J., Nixon, F.C., England, J.H.: New marine ΔR values for
858 Arctic Canada, **Quaternary Geochronology**, 5, 419–434, 2010.
- 859 [18] Cronin, T.M., Polyak, L., Reed, D., Kandiano, E.S., Marzen, R.E., Council, E.A.: A 600-ka Arctic sea-ice
860 record from Mendeleev Ridge based on ostracodes, **Quaternary Science Reviews**, 79, 157–167, 2013.
- 861 [19] Dalrymple, R.W. and Maass, O. C.: Clay mineralogy of late Cenozoic sediments in the CESAR cores,
862 Alpha Ridge, central Arctic ocean, **Canadian Journal of Earth Science**, 24, 1562–1569, 1987.
- 863 [20] Darby, D.A.: Kaolinite and other clay minerals in Arctic Ocean sediments, **Journal of Sedimentary**
864 **Petrology**, 45, 272–279, 1975.
- 865 [21] Darby, D. A., Bischof, J. F., Jones, G. A.: Radiocarbon chronology of depositional regimes in the western
866 Arctic Ocean, **Deep Sea Research Part II**, 44 (8), 1745–1757, 1997.
- 867 [22] Darby, D. A., Bischof, J. F., Spielhagen, R. F., Marshall, S. A., Herman, S. W.: Arctic ice export events
868 and their potential impact on global climate during the Late Pleistocene, **Paleoceanography**, 17(2), 1025,
869 doi:10.1029/2001PA000639, 2002.
- 870 [23] Darby, D. A.: Sources of sediment found in sea ice from the western Arctic Ocean, new insights into
871 processes of entrainment and drift patterns, **Journal of Geophysical Research**, 108(C8), 3257,
872 doi:10.1029/2002JC001350, 2003.
- 873 [24] Darby, D. A., and Bischof, J. F.: A Holocene record of changing Arctic Ocean ice drift, analogous to the
874 effects of the Arctic Oscillation, **Paleoceanography**, 19, PA1027, doi:10.1029/2003PA000961, 2004.
- 875 [25] Darby, D.A., Polyak, L., Bauch, H.A.: Past glacial and interglacial conditions in the Arctic Ocean and
876 marginal seas — a review, **Progress in Oceanography**, 71, 129–144, 2006.
- 877 [26] Darby, D. A., Ortiz, J., Polyak, L., Lund, S., Jakobsson, M., Woodgate, R.A.: The role of currents and sea



- 878 ice in both slowly deposited central Arctic and rapidly deposited Chukchi-Alaskan margin sediments,
879 **Global and Planetary Change**, 68, 58-72, 2009.
- 880 [27] Darby, D. A., Myers, W., Jakobsson, M., Rigor, I.: Modern dirty sea ice characteristics and sources: The
881 role of anchor ice, **Journal of Geophysical Research**, 116: C09008, doi:10.1029/2010JC006675, 2011.
- 882 [28] Darby, D., Ortiz, J., Grosch, C., Lund, S.: 1,500-year cycle in the Arctic Oscillation identified in
883 Holocene Arctic sea-ice drift. **Nature Geoscience** 5, 897–900, 2012.
- 884 [29] Dethleff, D. A., Rachold, V., Tintelnot, T., Antonow, M.: Sea-ice transport of riverine particles from the
885 Laptev Sea to Fram Strait based on clay mineral studies, **International Journal of Earth Science**, 89,
886 496–502, 2000.
- 887 [30] Dethleff, D.: Entrainment and export of Laptev Sea ice sediments, Siberian Arctic, **Journal of**
888 **Geophysical Research—Oceans** 110, C07009, doi:10.1029/2004JC002740, 2005.
- 889 [31] Dove, D., Polyak, L., Coakley, B.: Widespread, multi-source glacial erosion on the Chukchi margin,
890 Arctic Ocean, **Quaternary Science Reviews**, 92, 112-122, 2014.
- 891 [32] Dong, L., Shi, X., Liu, Y., Fang, X., Chen, Z., Wang, C., Zou, J., Huang, Y.: Mineralogical study of
892 surface sediments in the western Arctic Ocean and their implications for material sources, **Advances in**
893 **Polar Science**, 25(3), 192-203, 2014.
- 894 [33] Dowdeswell, J. A., Villinger, H., Whittington, R. J., Marienfeld, P.: Iceberg scouring in Scoresby Sund
895 and on the East Greenland continental shelf, **Marine Geology**, 111, 37–53, 1993.
- 896 [34] Dyke, A. S., Andrews, J. T., Clark, P. U., England, J. H., Miller, G. H., Shaw, J., Veillette, J. J.: The
897 Laurentide and Innuitian ice sheets during the Last Glacial Maximum, **Quaternary Science Review**, 21,
898 9–31, 2002.
- 899 [35] England, J.H., Furze, M.F.A., Doupe, J. P.: Revision of the NW Laurentide Ice Sheet: implications for
900 paleoclimate, the northeast extremity of Beringia, and Arctic Ocean sedimentation, **Quaternary Science**
901 **Review**, 28, 1573-1596, 2009.
- 902 [36] Fagel, N., Not, C., Gueibe, J., Mattielli, N., Bazhenova, E.: Late Quaternary evolution of sediment
903 provenances in the Central Arctic Ocean: mineral assemblage, trace element composition and Nd and Pb
904 isotope fingerprints of detrital fraction from the Northern Mendeleev Ridge, **Quaternary Science**
905 **Reviews**, 92, 140-154, 2014.
- 906 [37] Grosswald, M.G. and Hughes, T.J.: The Russian component of an Arctic Ice Sheet during the Last Glacial
907 Maximum, **Quaternary Science Review**, 21, 121-146, 2002.



- 908 [38] Haley, B.A. and Polyak, L.: Pre-modern Arctic Ocean circulation from surface sediment neodymium
909 isotopes, **Geophys. Res. Lett.**, 40, 1–5, 2013.
- 910 [39] Hanslik, D., Jakobsson, M., Backman, J., Björck, S., Sellén, E., O'Regan, M., Fornaciari, E., Skog, G.:
911 Quaternary Arctic Ocean sea ice variations and radiocarbon reservoir age corrections, **Quaternary**
912 **Science Reviews**, 29, 3430–3441, 2010.
- 913 [40] Head, M.J. and Gibbard, P. L.: Early-Middle Pleistocene transitions: linking terrestrial and marine realms,
914 **Quaternary International**, 389, 7–46, 2015.
- 915 [41] Hebbeln, D.: Flux of ice-rafted detritus from sea ice in the Fram Strait, **Deep-Sea Research Part II**, 47,
916 1773–1790, 2000.
- 917 [42] Hesse, R. and Khodabakhsh, S.: Anatomy of Labrador Sea Heinrich layers, **Marine Geology**, 380, 44–66,
918 2016.
- 919 [43] Hughes, T.J., Denton, G.H., Grosswald, M.G.: Was there a late-Würm Arctic ice sheet? **Nature**, 266,
920 596–602, 1977.
- 921 [44] Jakobsson, M., Løvlie, R., Al-Hanbali, H., Arnold, E., Backman, J., Mörth, M.: Manganese and color
922 cycle in Arctic Ocean sediments constrain Pleistocene chronology, **Geology**, 28, 23–26, 2000.
- 923 [45] Jakobsson, M., Polyak, L., Edwards, M., Kleman, J., Coakley, B.: Glacial geomorphology of the Central
924 Arctic Ocean: the Chukchi Borderland and the Lomonosov Ridge, **Earth Surface Processes and**
925 **Landforms**, 33, 526–545, 2008.
- 926 [46] Jakobsson, M., Andreassen, K., Bjarnadóttir, L. R., Dove, D., Dowdeswell, J. A., England, J.H., Funder,
927 S., Hogan, K., Ingólfsson, Ó., Jennings, A., Larsen, N, K., Kirchner, N., Landvik, J.Y., Mayer, L.,
928 Mikkelsen, N., Möller, P., Niessen, F., Nilsson, J., O'Regan, M., Polyak, L., Nørgaard-Pedersen, N.,
929 Stein, R.: Arctic Ocean glacial history, **Quaternary Science Reviews**, 92, 40–67, 2014.
- 930 [47] Jakobsson, M., Nilsson, J., Anderson, L., Backman, J., Björck, G., Cronin, T.M., Kirchner, N.,
931 Koshurnikov, A., Mayer, L., Noormets, R., O'Regan, M., Stranne, C., Ananiev, R., Macho, N. B.,
932 Cherniykh, D., Coxall, H., Eriksson, B., Flodén, T., Gemery, L., Gustafsson, O., Jerram, K., Johansson, C.,
933 Khortov, A., Mohammad, R., Semiletov, I.: Evidence for an ice shelf covering the central Arctic Ocean
934 during the penultimate glaciation, **Nature Communications**, doi: 10.1038/ncomms10365, 2016.
- 935 [48] Jang, K., Han, Y., Huh, Y., Nam, S., Stein, R., Mackensen, A., Matthiessen, J.: Glacial freshwater
936 discharge events recorded by authigenic neodymium isotopes in sediments from the Mendeleev Ridge,
937 western Arctic Ocean, **Earth and Planetary Science Letters**, 369–370, 148–157, 2013.



- 938 [49] Junttila, J.: Clay minerals in response to Mid-Pliocene glacial history and climate in the polar regions
939 (ODP, Site 1165, Prydz Bay, Antarctica and Site 911, Yermak Plateau, Arctic Ocean), **Acta Universitat**
940 **Ouluensis**, A 481, 2007.
- 941 [50] Kalinenko, V.V.: Clay minerals in sediments of the Arctic Seas. **Lithology and Mineral Resources**, 36,
942 362–372, 2001.
- 943 [51] Kaparulina, E., Strand, K., Lunkka, J. P.: Provenance analysis of central Arctic Ocean sediments:
944 Implications for circum-Arctic ice sheet dynamics and ocean circulation during Late Pleistocene,
945 **Quaternary Science Reviews**, XXX, 1–11, 2015.
- 946 [52] Keigwin, L.D., Donnelly, J.P., Cook, M.S., Driscoll, N.W., Brigham-Grette, J.: Rapid sea-level rise and
947 Holocene climate in the Chukchi Sea, **Geology**, 34 (10), 861–864, doi:10.1130/G22712.1, 2006.
- 948 [53] Kim, B.I. and Slobodin, V.Ya.: Main stages of the evolution of East Arctic shelves of Russia and
949 Canadian Arctic in the Paleogene and Neogene, **In: Geologiya skladchatogo obramleniya**
950 **Ameraziiskogo subbasseina (Geology of the Folded Framing of the Amerasian Subbasin)**, St.
951 Petersburg: Sevmorgeologiya, 104–116, 1991.
- 952 [54] Knies, J., Kleiber, H. P., Matthiessen, J., Müller, C., Nowaczyk, N.: Marine ice-rafted debris records
953 constrain maximum extent of Saalian and Weichselian ice-sheets along the northern Eurasian margin,
954 **Global and Planetary Change**, 31, 45–64, 2001.
- 955 [55] Knies, J. and Vogt, C.: Freshwater pulses in the eastern Arctic Ocean during Saalian and early
956 Weichselian ice-sheet collapse, **Quaternary Research**, 60, 243–251, 2003.
- 957 [56] Kobayashi, D., Yamamoto, M., Tirino, T., Nam, S.-I., Park, Y.-H., Harada, N., Nagashima, K., Chikita,
958 K., Saitoh, S.I.: Distribution of detrital minerals and sediment color in western Arctic Ocean and
959 northern Bering Sea sediments: changes in the provenance of western Arctic Ocean sediments since the
960 last glacial period, **Polar Science**, 10, 519–531, 2016.
- 961 [57] Krylov, A. A., Andreeva I. A., Vogt C., Backman J., Krupskaya V. V., Grikurov G. E., Moran K., Shoji H.:
962 A shift in heavy and clay mineral provenance indicates a middle Miocene onset of a perennial sea ice
963 cover in the Arctic Ocean, **Paleoceanography**, 23, PA1S06, doi:10.1029/2007PA001497, 2008.
- 964 [58] Krylov, A.A., Stein, R., Ermakova, L.A. Clay minerals as indicators of late quaternary sedimentation
965 constraints in the Mendeleev Rise, Amerasian Basin, Arctic Ocean, **Lithology and Mineral Resources**,
966 49, 103–116, 2014.
- 967 [59] Larsen, E., Kjær, K.H., Demidov, I.N., Funder, S., Grøsfjeld, K., Houmark-Nielsen, M., Jensen, M.,



- 968 Linge, H., Lyså, A.: Late Pleistocene glacial and lake history of northwestern Russia, **Boreas**, 35,
969 394-424, 2006.
- 970 [60] Lazar, K.B. and Polyak, L.: Pleistocene benthic foraminifers in the Arctic Ocean: Implications for seaice
971 and circulation history, **Marine Micropaleontology**, 126, 19-30, 2016.
- 972 [61] Löwemark, L., März, C., O'Regan, M., Gyllencreutz, R. Arctic Ocean Mn-stratigraphy: genesis,
973 synthesis and inter-basin correlation, **Quaternary Science Reviews**, 92, 97-111, 2014.
- 974 [62] Margold M., Stokes C. R., Clark C. D.: Ice streams in the Laurentide Ice Sheet: Identification,
975 characteristics and comparison to modern ice sheets, **Earth-Science Reviews**, 143, 117-146, 2015.
- 976 [63] März, C., Stratmann, A., Matthiessen, J., Meinhardt, A., Eckert, S., Schnetger, B., Vogt, C., Stein, R.,
977 Brumsack, H.: Manganese-rich brown layers in Arctic Ocean sediments: composition, formation
978 mechanisms, and diagenetic overprint. **Geochimica et Cosmochimica Acta**, 75, 7668-7687, 2011.
- 979 [64] Matthiessen, J., Niessen F., Stein, R., Naafs, B. D.: Pleistocene Glacial Marine Sedimentary
980 Environments at the Eastern Mendeleev Ridge, Arctic Ocean, **Polarforschung**, 79 (2), 123 – 137, 2009
981 (erschienen 2010).
- 982 [65] Naidu, A.S., Burrell, D.C., Hood, D.W.: Clay mineral composition and geological significance of some
983 Beaufort Sea sediments, **Journal of Sedimentary Petrology**, 41, 691-694, 1971.
- 984 [66] Naidu, A. S., Creager, J. S., Mowatt, T. C.: Clay mineral dispersal patterns in the north Bering and
985 Chukchi Seas. **Marine Geology**, 47(1), 1-15, 1982.
- 986 [67] Niessen, F., Hong, J.K., Hegewald, A., Matthiessen, J., Stein, R., Kim, H., Kim, S., Jensen, L., Jokat, W.,
987 Nam, S.-I., Kang, S.-H.: Repeated Pleistocene glaciation of the East Siberian Continental Margin,
988 **Nature Geoscience**, 6, 842-846, 2013.
- 989 [68] Nürnberg, D., Wollenburg, I., Dethleff, D., Eicken, H., Kassens, H., Letzig, T., Reimnitz, E., Thiede, J.:
990 Sediments in Arctic sea ice: Implications for entrainment, transport and release, **Marine Geology**, 119,
991 185-214, 1994.
- 992 [69] Nwaodua, E.C., Ortiz J. D., Griffith E. M.: Diffuse spectral reflectance of surficial sediments indicates
993 sedimentary environments on the shelves of the Bering Sea and western Arctic, **Marine Geology**, 355,
994 218-233, 2014.
- 995 [70] O'Regan, M., King, J., Backman, J., Jakobsson, M., Pälike, H., Moran, K., Heil, C., Sakamoto, T., Cronin,
996 T.M., Jordan, R.W.: Constraints on the Pleistocene chronology of sediments from the Lomonosov Ridge,
997 **Paleoceanography**, 23, PA1S19, doi:10.1029/2007PA001551, 2008.



- 998 [71] Ortiz, J.D., Polyak, L., Grebmeier, J.M., Darby, D., Eberl, D.D., Naidu, S., Nof, D.: Provenance of
999 Holocene sediment on the Chukchi–Alaskan margin based on combined diffuse spectral reflectance and
1000 quantitative X-Ray diffraction analysis, **Global and Planetary Change**, 68 (no. 1–2), 73–84, 2009.
- 1001 [72] Phillips, R. L. and Grantz, A.: Regional variations in provenance and abundance of ice-rafted clasts in
1002 Arctic Ocean sediments: Implications for the configuration of late Quaternary oceanic and atmospheric
1003 circulation in the Arctic, **Marine Geology**, 172, 91–115, 2001.
- 1004 [73] Poirier, R.K., Cronin, T.M., Briggs Jr., W.M., Lockwood, R.: Central Arctic paleoceanography for the last
1005 50 kyr based on ostracode faunal assemblages, **Marine Micropaleontology**, 88–89, 65–76, 2012.
- 1006 [74] Polyak, L., Edwards, M.H., Coakley, B.J., Jakobsson, M.: Ice shelves in the Pleistocene Arctic Ocean
1007 inferred from glaciogenic deep-sea bedforms, **Nature**, 410, 453–459, 2001.
- 1008 [75] Polyak, L. V., Curry, W. B., Darby, D. A., Bischof, J., Cronin, T. M.: Contrasting glacial/interglacial
1009 regimes in the Western Arctic Ocean as exemplified by a sedimentary record from the Mendeleev Ridge,
1010 **Palaeogeography, Palaeoclimatology, Palaeoecology**, 203, 73–93, 2004.
- 1011 [76] Polyak, L., Darby, D.A., Bischof, J., Jakobsson, M.: Stratigraphic constraints on late Pleistocene glacial
1012 erosion and deglaciation of the Chukchi margin, Arctic Ocean, **Quaternary Research**, 67:234–245,
1013 doi:10.1016/j.yqres.2006.08.001, 2007.
- 1014 [77] Polyak, L., Bischof, J., Ortiz, J.D., Darby, D.A., Channell, J.E.T., Xuan, C., Kaufman, D.S., Lovlie, R.,
1015 Schneider, D.A., Eberl, D.D., Adler, R.E., Council, E.A.: Late Quaternary stratigraphy and sedimentation
1016 patterns in the western Arctic Ocean, **Global and Planetary Change**, 68, 5–17, 2009.
- 1017 [78] Polyak, L., Alley, R.B., Andrews, J.T., Brigham-Grette, J., Cronin, T.M., Darby, D.A., Dyke, A.S.,
1018 Fitzpatrick, J.J., Funder, S., Holland, M., Jennings, A.E., Miller, G.H., O’Regan, M., Savelle, J., Serreze,
1019 M., St. John, K., White, J.W.C., Wolff, E.: History of sea ice in the Arctic, **Quaternary Science Reviews**,
1020 29, 1757–1778, 2010.
- 1021 [79] Polyak, L., Best, K. M., Crawford, K. A., Council, E. A., St-Onge, G.: Quaternary history of sea ice in the
1022 western Arctic Ocean based on foraminifera, **Quaternary Science Reviews**, 79, 145–156, 2013.
- 1023 [80] Ramaswamy V. and Rao P. S.: Grain Size Analysis of Sediments from the Northern Andaman Sea:
1024 Comparison of Laser Diffraction and Sieve-Pipette Techniques, **Journal of Coastal Research**, 22,
1025 1000–1009, 2006.
- 1026 [81] Rigor, I.G., Wallace, J.M., Colony, R.L.: Response of sea ice to the Arctic Oscillation, **Journal of**
1027 **Climate**, 15, 2648–2663, 2002.



- 1028 [82] Rudels, B.: Arctic Ocean circulation. **Encyclopedia of Ocean Sciences**, J.H. Steele, K.K. Turekian,
1029 S.A. Thorpe (Eds.-in-Chief), Elsevier, 211-225, 2009.
- 1030 [83] Sharma, M., Basu, A.R., Nesterenko, G. V.: Temporal Sr-, Nd- and Pb isotopic variations in the Siberian
1031 flood basalts: implications for the plume-source characteristics, **Earth and Planetary Science Letters**,
1032 113, 365-381, 1992.
- 1033 [84] Slobodin, V.Ya., Kim, B.I., Stepanova, G.V., Kovalenko, F.Ya.: Differentiation of the Aion borehole
1034 section based on the biostratigraphic data, **In: Stratigrafiya i paleontologiya mezo-kainozoya**
1035 **Sovetskoi Arktiki (Stratigraphy and Paleontology of the Meso-Cenozoic in the Soviet Arctic)**,
1036 Leningrad: Sevmergeologiya, 43–58, 1990.
- 1037 [85] Spielhagen, R. F., Bonani, G., Eisenhauer, A., Frank, M., Frederichs, T., Kassens, H., Kubik, P. W.,
1038 Mangini, A., Nørgaard-Pedersen, N., Nowaczyk, N. R., Schäper, S., Stein, R., Thiede, J., Tiedemann, R.,
1039 Wahsner, M.: Arctic Ocean evidence for Late Quaternary initiation of northern Eurasian ice sheets,
1040 **Geology**, 25, 783–786, 1997.
- 1041 [86] Spielhagen, R. F., Baumann, K. H., Erlenkeuser, H., Nowaczyk, N. R., Nørgaard-Pedersen, N., Vogt, C.,
1042 Weiel, D. Arctic Ocean deep-sea record of Northern Eurasian ice sheet history, **Quaternary Science**
1043 **Review**, 23, 1455–1483, 2004.
- 1044 [87] Schoster, F., Behrends, M., Müller, C., Stein, R., Wahsner, M.: Modern river discharge in the Eurasian
1045 Arctic Ocean: Evidence from mineral assemblages and major and minor element distributions,
1046 **International Journal of Earth Science**, 89, 486–495, 2000.
- 1047 [88] Sellén, E., O'Regan, M., Jakobsson, M.: Spatial and temporal Arctic Ocean depositional regimes: a key
1048 to the evolution of ice drift and current patterns, **Quaternary Science Reviews**, 29, 3644-3664, 2010.
- 1049 [89] Stärz, M., Gong, X., Stein, R., Darby, D.A., Kauker, F., Lohmann, G.: Glacial shortcut of Arctic sea-ice
1050 transport, **Earth and Planetary Science Letters**, 357–358, 257–267, 2012.
- 1051 [90] Stein, R., Grobe, H., Wahsner, M.: Organic carbon, carbonate, and clay mineral distributions in eastern
1052 central Arctic Ocean surface sediments, **Marine Geology**, 119, 269-285, 1994.
- 1053 [91] Stein R.: Arctic Ocean Sediments: Processes, Proxies, and Paleoenvironment, **Elsevier**, Amsterdam,
1054 1-592 pp, 2008.
- 1055 [92] Stein, R., Matthiessen, J., Niessen, F.: Re-Coring at Ice Island T3 Site of Key Core FL-224 (Nautilus
1056 Basin, Amerasian Arctic): Sediment Characteristics and Stratigraphic Framework, **Polarforschung**, 79
1057 (2), 81 – 96, 2010a.



- 1058 [93] Stein, R., Matthiessen, J., Niessen, F., Krylov, A., Nam, S., Bazhenova, E., Shipboard Geology Group.:
 1059 Towards a better (litho-) stratigraphy and reconstruction of Quaternary paleoenvironment in the
 1060 Amerasian Basin (Arctic Ocean), **Polarforschung**, 79 (2), 97–121, 2010b.
- 1061 [94] Stein, R., Fahl, K., Müller J.: Proxy Reconstruction of Cenozoic Arctic Ocean Sea-Ice History– from
 1062 IRD to IP25, **Polarforschung**, 82 (1), 37–71, 2012.
- 1063 [95] Stokes, C.R., Clark, C.D., Darby, D., Hodgson, D.A.: Late Pleistocene ice export events into the Arctic
 1064 Ocean from the M'Clure Strait Ice Stream, Canadian Arctic Archipelago, **Global and Planetary Change**,
 1065 49, 139–162, 2005.
- 1066 [96] Stokes, C.R., Clark, C.D., Storrar, R.: Major changes in ice stream dynamics during deglaciation of the
 1067 north-western margin of the Laurentide Ice Sheet, **Quaternary Science Reviews**, 28, 721–738, 2009.
- 1068 [97] Svendsen, J. I., Alexanderson, H., Astakhov, V. I., Demidov, I., Dowdeswell, J. A., Funder, S., Gataullin,
 1069 V., Henriksen, M., Hjort, C., Houmark-Nielsen, M., Hubberten, H. W., Ingólfsson, O., Jakobsson, M.,
 1070 Kjær, K. H., Larsen, E., Lokrantz, H., Lunkka, J. P., Lyså, A., Mangerud, J., Mamioukhov, A., Murray, A.,
 1071 Möller, P., Niessen, F., Nikolskaya, O., Polyak, L., Saarnisto, M., Siegert, R., Siegert, M. J., Spielhagen,
 1072 R. F., Stein, R.: Late Quaternary ice sheet history of Northern Eurasia, **Quaternary Science Review**, 23,
 1073 1229–1271, 2004.
- 1074 [98] Vogt, C.: Regional and temporal variations of mineral assemblages in Arctic Ocean sediments as climatic
 1075 indicator during glacial/interglacial changes, **Report on Polar Marine Research**, 251, 309, 1997.
- 1076 [99] Vogt, C., Knies, J., Spielhagen, R. F., Stein, R.: Detailed mineralogical evidence for two nearly identical
 1077 glacial/deglacial cycles and Atlantic water advection to the Arctic Ocean during the last 90,000 years,
 1078 **Global and Planetary Change**, 31, 23–44, 2001.
- 1079 [100] Vogt, C. and Knies, J.: Sediment dynamics in the Eurasian Arctic Ocean during the last deglaciation —
 1080 The clay mineral group smectite perspective, **Marine Geology**, 250, 211–222, 2008.
- 1081 [101] Vogt, C. and Knies, J.: Sediment pathways in the western Barents Sea inferred from clay mineral
 1082 assemblages in surface sediments, **Norwegian Journal of Geology**, 89, 41–55, 2009.
- 1083 [102] Viscosi-Shirley, C., Mammone, K., Piasias, N., Dymond, J.: Clay mineralogy and multi-element chemistry
 1084 of surface sediments on the Siberian-Arctic shelf: Implications for sediment provenance and grain size
 1085 sorting, **Continental Shelf Research**, 23, 1175–1200, 2003.
- 1086 [103] Wahsner, M., Müller, C., Stein, R., Ivanov, G., Levitan, M., Shelekova, E., Tarasov, G.: Clay mineral
 1087 distributions in surface sediments from the Central Arctic Ocean and the Eurasian continental margin as



- 1088 indicator for source areas and transport pathways: a synthesis, **Boreas**, 28, 215-233, 1999.
- 1089 [104] Wang, D. and Hesse, R.: Continental slope sedimentation adjacent to an ice-margin. II. Glaciomarine
1090 depositional facies on Labrador Slope and glacial cycles, **Marine Geology**, 135, 65-96, 1996.
- 1091 [105] Wang, R., Xiao, W., März, C., Li, Q.: Late Quaternary paleoenvironmental changes revealed by
1092 multi-proxy records from the Chukchi Abyssal Plain, western Arctic Ocean, **Global and Planetary
1093 Change**, 108, 100–118, 2013.
- 1094 [106] Winkler, A., Wolf-Welling, T.C.W., Stattegger, K., Thiede, J.: Clay mineral sedimentation in high
1095 northern latitude deep-sea basins since the Middle Miocene (ODP Leg 151, NAAG), **International
1096 Journal of Earth Sciences**, 91,133–148, 2002.
- 1097 [107] Winter, B.L., Johnson, C.M., Clark, D.L.: Strontium, neodymium, and lead isotope variations of
1098 authigenic and silicate sediment components from the Late Cenozoic Arctic Ocean: implications for
1099 sediment provenance and the source of trace metals in seawater, **Geochimica et Cosmochimica Acta**, 61,
1100 4181-4200, 1997.
- 1101 [108] Xiao, W., Wang, R., Polyak, L., Astakhov, A., Cheng, X.: Stable oxygen and carbon isotopes in
1102 planktonic foraminifera *Neogloboquadrina pachyderma* in the Arctic Ocean: an overview of published
1103 and new surface-sediment data, **Marine Geology**, 352, 397-408, 2014.
- 1104 [109] Xuan, C. and Channell, J.E.T.: Origin of apparent magnetic excursions in deep-sea sediments from
1105 Mendeleev-Alpha Ridge (Arctic Ocean), **Geochemistry, Geophysics, Geosystems**, 11, Q02003, 2010.
- 1106 [110] Yurco, L. N., Ortiz, J. D., Polyak, L., Darby, D. A., Crawford, K. A.: Clay mineral cycles identified by
1107 diffuse spectral reflectance in Quaternary sediments from the Northwind Ridge: implications for
1108 glacial–interglacial sedimentation patterns in the Arctic Ocean, **Polar Research**, 29, 176–197, 2010.
- 1109 [111] Zou, H.: An X-ray diffraction approach: bulk mineral assemblages as provenance indicator of sediments
1110 from the Arctic Ocean, PhD Thesis, University of Bremen, Bremen, 1-104 pp, 2016.
1111



1112 **Table 1.** Minerals Actively Sought in Diffraction Data Analysis

1113

Mineral	window(°2θ, CuKα radiation)	Range of D-Spacing(A)	Intensity Factor
Amphibole	10.30-10.70	8.59- 8.27	2.5
Augite	29.70-30.00	3.00- 2.98	5
Calcite	29.25-29.60	3.04- 3.01	1.65
Chlorite	18.50-19.10	4.79- 4.64	4.95
Dolomite	30.80-31.15	2.90- 2.87	1.53
K-Feldspar	27.35-27.79	3.26- 3.21	4.3
Quartz	26.45-26.95	3.37- 3.31	1

1114



1115 **Table 2.** AMS¹⁴C datings in core BN05.

1116

Sample no.	Depth (cm)	AMS 14C age (14C a BP)	Calibrated age median (cal yr BP)	2-σ range (cal yr BP)
112767	4-6	7810±35	7885	7797-7958
112768	8-10	8180±35	8259	8171-8340
112769	18-20	38600±300	41703	41202-42165
115944	22-24	40800±410	43140	42522-43901

1117



1118 **Table 3.** Characterization and interpretation of sedimentary variable groups (Fig. 6)

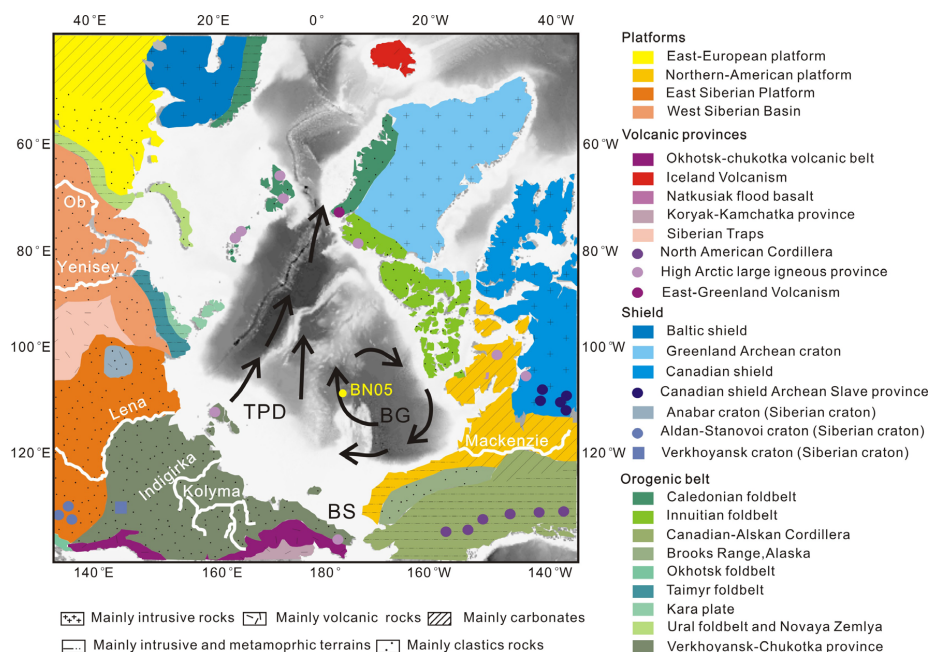
1119

Group	Leading/ opposite proxies	Environments	Depositional processes	Provenance
1	Foraminifers, calcite, Mn, clay/ coarse grains (esp. silt), quartz	Interglacial (incl. major interstadials)	Sea ice	Mixed
2	Dolomite, Ca, Qua/Fsp / plagioclase, pyroxene, feldspar	Glacial/ deglacial	Icebergs, meltwater	North American
3	Feldspar, pyroxene, plagioclase/ Ca, dolomite, Qua/Fsp	Interglacial/ deglacial	Sea ice, icebergs	Siberian
4	Smectite, kaolinite, chlorite / clay	Glacial/ deglacial	Icebergs, debris flows	E Siberian
5, 6	Coarse grains (incl. silt)	Glacial/ deglacial	Icebergs, debris flows	Mixed

1120



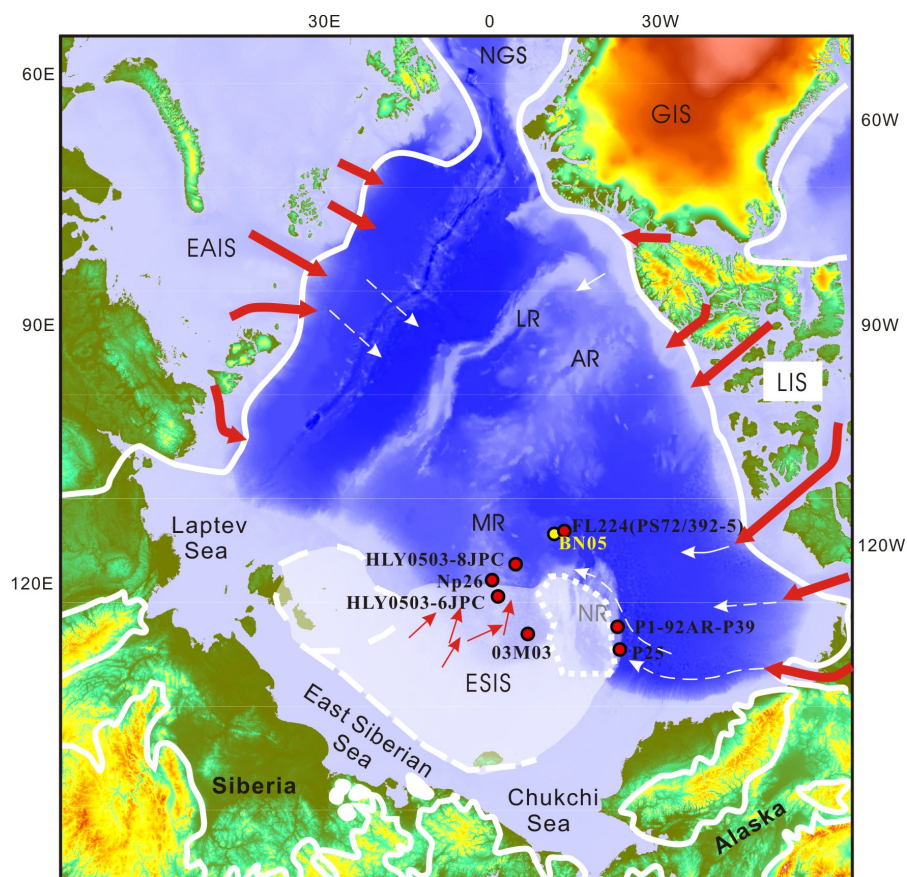
1121



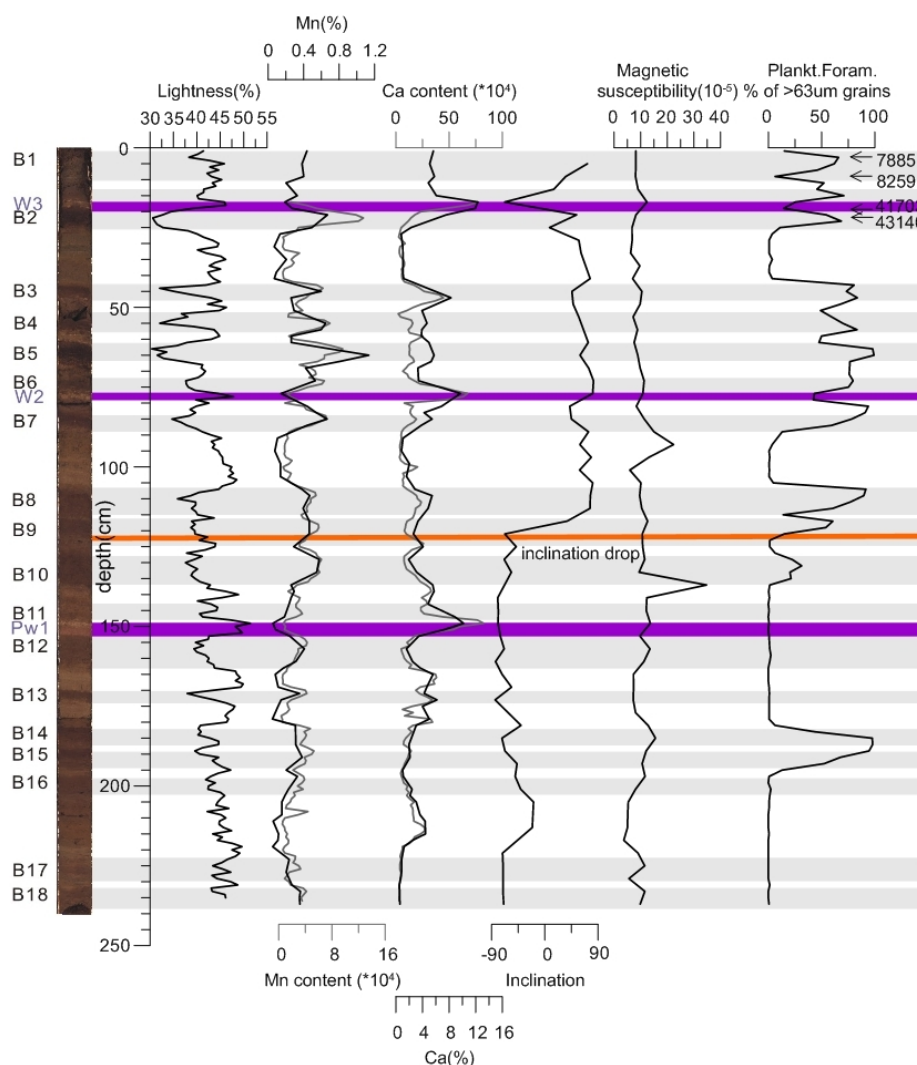
1122

1123

1124 **Figure 1.** Background map showing the location of core ARC4-BN05, the main
 1125 Arctic rivers and the two major surface current systems: Beaufort Gyre (BG) and
 1126 Transpolar Drift (TPD). Schematic geological map shows the distribution and
 1127 prevailing lithology of the main terrains adjacent to the Arctic Ocean (Fagel et al.,
 1128 2014).



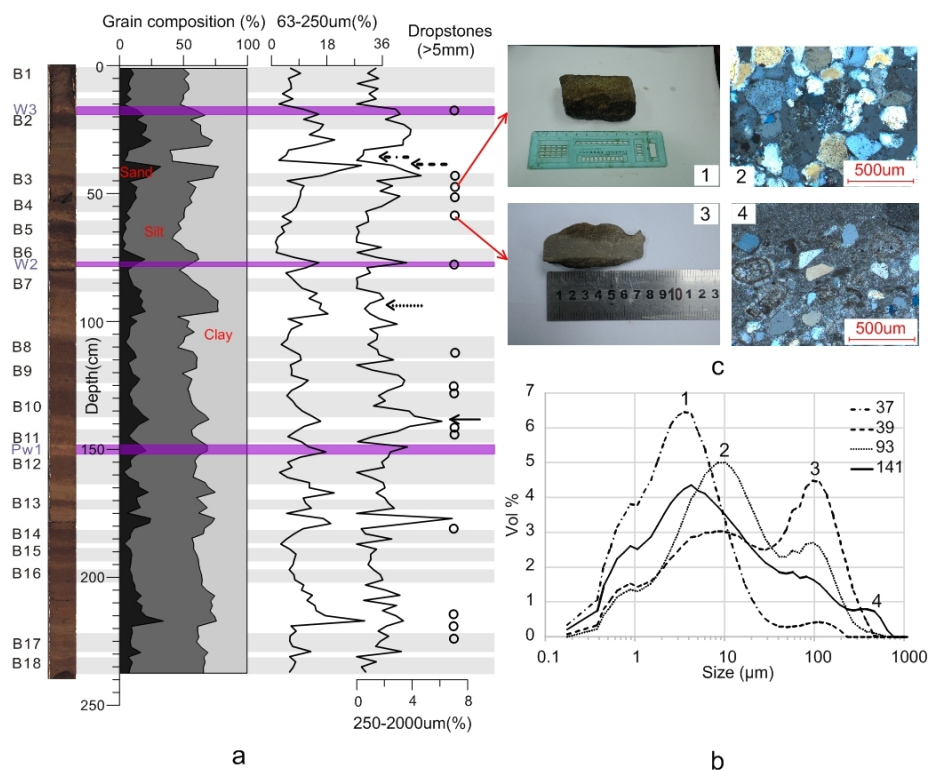
1129
1130 **Figure 2.** Index map showing the location of core ARC4-BN05 (yellow circle) and
1131 other cores from previous studies mentioned in this paper (red circles). LR, MR, AR,
1132 and NR are Lomonosov, Mendeleev, Alpha, and Northwind ridges, respectively; NGS
1133 is Norwegian–Greenland Sea. White lines show maximal Pleistocene limits
1134 reconstructed for Greenland, Laurentide, Eurasian, and East Siberian Ice Sheets (GIS,
1135 LIS, EAIS and ESIS; England et al., 2009; Svendsen et al., 2004; Niessen et al., 2013).
1136 Proposed flow lines for grounded ice sheets and ice shelves (red and white arrows,
1137 respectively) are after Niessen et al. (2013).
1138



1139
 1140 **Figure 3.** Lithostratigraphy and major proxies in core BN05: core photograph with
 1141 brown layer indices, lightness, Ca and Mn content (bulk XRF –grey line, ICP-OES –
 1142 black line), paleomagnetic inclination, planktic foraminiferal abundance, and AMS¹⁴C
 1143 datings. Predominantly dark brown intervals B1-B18 are highlighted in grey; high-Ca,
 1144 pink-white layers are marked by purple lines. The main inclination drop is marked by
 1145 orange line. See Table S1 for data used.

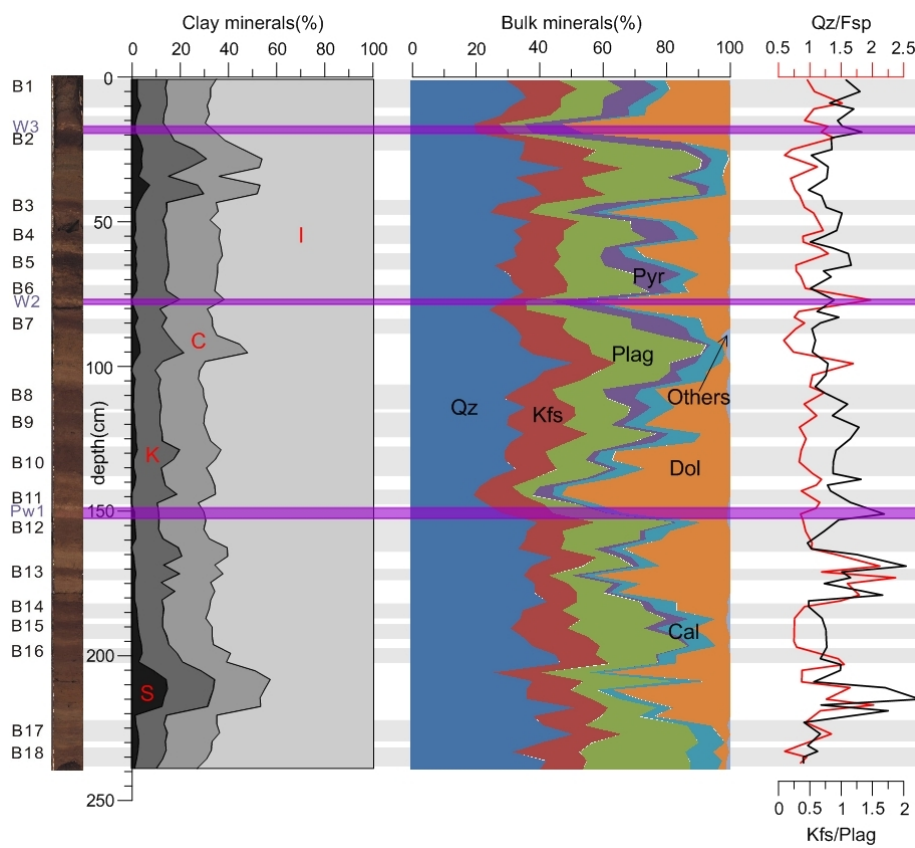


1146



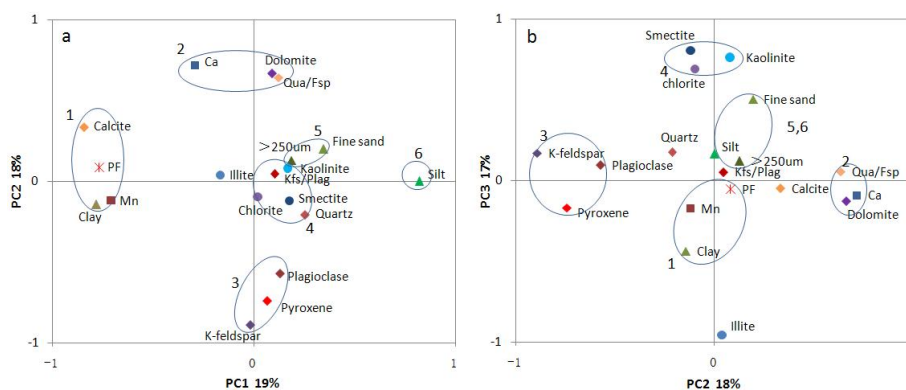
1147

1148 **Figure 4. (a)** Down-core grain-size distribution in core ARC4-BN05: clay (<4 µm),
 1149 silt (4-63 µm), sand (63-2000 µm), fine sand (63-250 µm), and coarser sediment
 1150 (250-2000µm). Occurrence of dropstones >5 mm is shown by circles on the right. See
 1151 Fig. 3 for lithostratigraphy explanation, and Tables S1-2 for data used. **(b)**
 1152 Granulometric distribution types exemplifying major grain-size modes 1-4. Position
 1153 of respective curves in core ARC4-BN05 is indicated in the legend (depth in core, cm)
 1154 and is shown by arrows in panel **a**. **(c)** Examples of dropstones from core
 1155 ARC4-BN05. 1, 48-54 cm, quartz sandstone; 2, same dropstone, thin section in cross
 1156 polarized light; 3, 56-63.5 cm, dolomite dropstone; 4, same dropstone, thin section in
 1157 cross polarized light.



1158

1159 **Figure 5.** Relative weight contents of major clay mineral groups in the clay fraction
1160 ($<2 \mu\text{m}$), bulk mineral composition and related indices in core ARC4-BN05. S, K, C,
1161 and I indicate smectite, kaolinite, chlorite, and illite, respectively. Qz, Kfs, Plag, Pyr,
1162 Cal, and Dol are quartz, K-feldspar, plagioclase, pyroxene, calcite, and dolomite,
1163 respectively. See Fig. 3 for lithostratigraphy explanation and Table S1 for data used.



1164

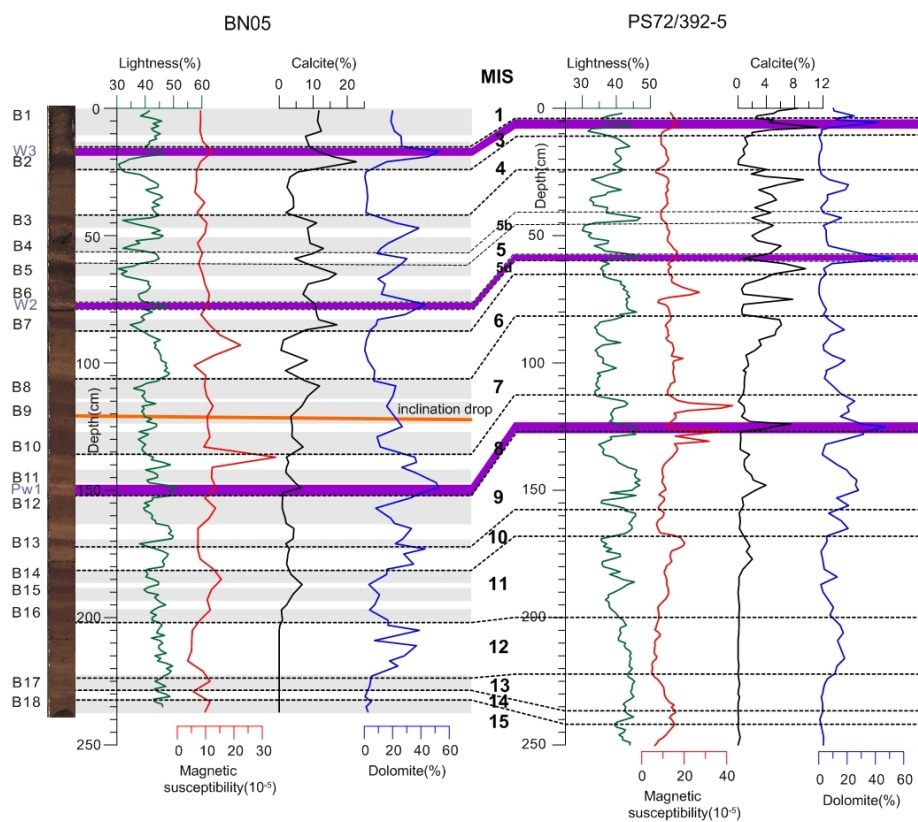
1165 **Figure 6.** Biplots of Principal Component loading scores in PC 1-2 (a) and PC 2-3 (b)

1166 space. Sedimentary variable groups or end members revealed by the loading

1167 distribution are enclosed by ellipses and numbered (see Table 3 and text in section 5.2

1168 for discussion). See Tables S3-4 for correlation between variables and PC loading

1169 scores.



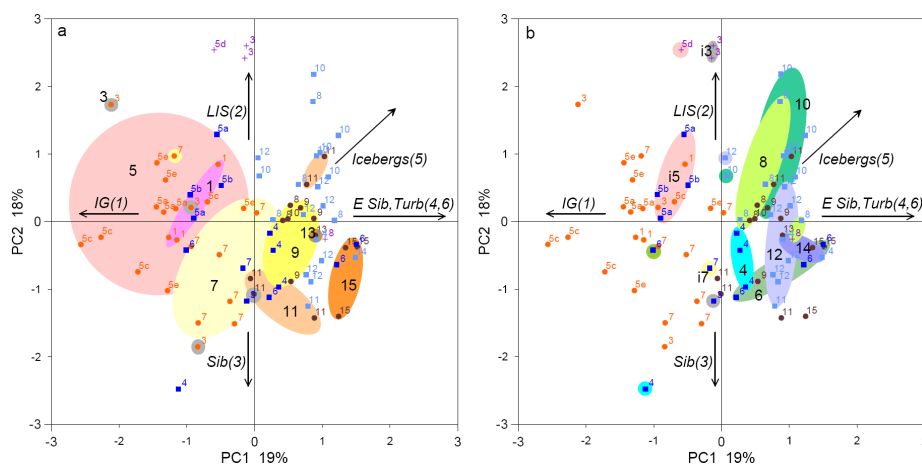
1170

1171 **Fig. 7.** Stratigraphic correlation of core BN05 with PS72/392-5 (Stein et al., 2010a)

1172 based on sediment lightness, magnetic susceptibility, calcite and dolomite content.

1173 See Fig. 3 for lithostratigraphy explanation.

1174



1175

1176 **Figure 8.** Biplots of downcore PC scores in the PC 1-2 space grouped by interglacial

1177 (a) and glacial intervals (b). Interpretation of loading score distribution: IG –

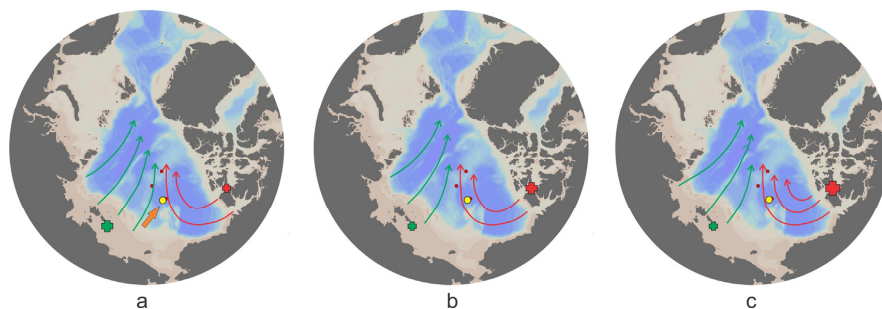
1178 interglacial environments, LIS – Laurentide Ice Sheet provenance, Sib/E Sib –

1179 Siberian/East Siberian provenance, Turb. – turbidites; variable group numbers shown

1180 in parentheses (Fig. 6; Table 3; see Section 5.2 above for more discussion). Numbers

1181 for individual and grouped samples show Marine Isotope Stages. See Table S5 for

1182 downcore PC score distribution.



1183
1184 **Figure 9.** Schematic reconstruction of glacial environments in the western Arctic
1185 Ocean and factors controlling sedimentation at the BN05 site (yellow circle): surface
1186 circulation (red and green arrows), glacioturbidites (orange filled arrow), and
1187 ice-sheet size (red and green crosses). See Fig. 1 for modern circulation. (a) High
1188 ESIS inputs: MIS 4, 6, 12, and 14; (b) high LIS inputs: MIS 8 and 10; (c) especially
1189 high LIS inputs: intra-MIS5 and 3.